NUMERICAL MODELING OF CO_2-WATER-ROCK INTERACTIONS IN THE FARNSWORTH, TEXAS HYDROCARBON UNIT, USA

A Thesis

presented to

the Faculty of the Graduate School

at the University of Missouri, Columbia

In Partial Fulfillment

of the Requirements for the Degree

Master of Science

---

by

Bulbul Ahmmed

Dr. Martin S. Appold, Thesis Supervisor

May, 2015

The undersigned, appointed by the dean of the Graduate School,

have examined the thesis entitled

NUMERICAL MODELING OF CO_2-WATER-ROCK INTERACTIONS IN THE FARNSWORTH, TEXAS HYDROCARBON UNIT, USA

Presented by Bulbul Ahmmed,

A candidate for the degree of Masters of Science

And hereby certify that, in their opinion, it is worthy of acceptance.

Dr. Martin S. Appold

Dr. Peter I. Nabelek

Dr. Baolin Deng

ACKNOWLEDGMENTS

At first, I would like to thank my advisor to whom I am very much indebted, Dr. Martin Appold, whose mentorship, motivation, wisdom comments on various processes underwent during this work and generous co – operation from the very beginning has made successful completion of this thesis work. I am very much thankful to my thesis committee members, Dr. Peter I. Nabelek and Dr. Baolin Deng for their valuable time to be in my thesis committee and to provide feedbacks and suggestions for improvement of my thesis.

My thanks go to Dr. Brian J. O. L. McPherson of the University of Utah, Dr. Reid B. Grigg of the Petroleum Recovery Research Center at the New Mexico Institute of Mining and Technology, and Dr. Mark D. White of Pacific North National Laboratory for their input, comments, and suggestions to improve my thesis. I also want to thank William Ampomah, graduate student at New Mexico Institute of Mining and Technology, for his generous support with the geologic model. I am very grateful to Tianguang Fan, who performed the composition analyses of the Morrow B formation water.

I would like to thank the entire faculty, staff and my colleagues in the Department of Geological Sciences of MU for their support, encouragement and guidance. I also want to thank the Southwest Partnership on Carbon Sequestration and Chaparral Energy for their technical support. I also would like to acknowledge the U.S. Department of Energy for funding of this research under grant DE – FC26 – 05NT42591. Finally, I am very grateful to my loving parents who bless me all the time and my wife, Afroja Akter, who supports and encourages me in every minute.

TABLE OF CONTENTS

List of Figures

List of Tables

Abstract

Numerical speciation, reaction path, and reactive transport modeling were used to study the effects on pore water composition and mineralogy from CO_2 injection into the Pennsylvanian Morrow B Sandstone in the Farnsworth Unit in northern Texas to evaluate its potential for long-term CO_2 sequestration. Speciation modeling showed the present Morrow B formation water to be supersaturated with respect to an assemblage of zeolite, clay, carbonate, mica, and aluminum hydroxide minerals, and quartz. The principal accessory minerals in the Morrow B, feldspars and chlorite, were predicted to dissolve. A reaction path model in which CO_2 was progressively titrated up to its solubility limit into the Morrow B formation water showed the pH to decrease from its initial value of 7 to about 4.1 to 4.2, accompanied by the precipitation of small amounts of quartz, diaspore, and witherite. As the resultant CO_2-charged fluid reacted with more of the Morrow B mineral matrix, the pH rose, reaching a maximum of 5.1 to 5.2 at a water:rock ratio of 10:1. At a higher water:rock ratio of 100:1, the pH rose to only 4.6 to 4.7. Diaspore, quartz, and nontronite precipitated consistently regardless of the water:rock ratio, but the carbonate minerals, siderite, witherite, dolomite, and calcite, only precipitated at higher pH. As a result, CO_2 sequestration by mineral trapping was predicted to be important only at low water:rock ratios, accounting for a maximum of 2% of the titrated CO_2 at the lowest water:rock ratio investigated of 10:1, which corresponds to a small porosity increase of about 1.4 to 1.5%.

Reactive solute transport modeling extended the reaction path modeling by including the effects of multi-phase fluid flow, heat transport, and solute transport with the chemical reactions. CO_2 was injected at nine wells in the western part of the field for 10

years in the model simulations. During injection, fluid pressures near the wells rose from about 15 MPa to about 19.2 MPa, but quickly dissipated after injection ceased. A plume of immiscible CO_2 gas built up around the wells, reaching pore saturations of about 50%, but did not migrate far from the wells over time. In contrast, CO_2 dissolved into aqueous solution was transported to the eastern boundary of the field within 30 years. The pH in the aqueous CO_2 plume was as low as 4.74 and led to the dissolution of most of the native minerals in the Morrow B Sandstone matrix. Over the 30 years time of the simulations thus far, ankerite was the only carbonate mineral predicted to precipitate, and thus the only mineral sink for CO_2. Most of the injected CO_2 over the time frame of the simulations was predicted to be sequestered by hydrodynamic trapping, followed by solubility and mineral trapping, respectively. The amounts of mineral precipitation and dissolution were too small to affect the porosity and permeability significantly, meaning that the hydraulics of the aquifer should not be significantly affected by CO_2 injection.

PART I

CHEMICAL EFFECTS OF CO_2 SEQUESTRATION IN THE MORROW B SANDSTONE IN THE FARNSWORTH, TEXAS HYDROCARBON UNIT, U.S.A.

Introduction

The purpose of the present study was to evaluate the effects of CO_2 injection on the pore water and rock matrix composition of the Morrow B Sandstone member of the Upper Morrow Sandstone in the Farnsworth Unit (FWU) in northern Texas, USA. The Morrow B Sandstone in the Farnsworth Unit has been chosen as a site for commercial-scale CO_2 injection and enhanced hydrocarbon recovery by the U.S. Department of Energy's Southwest Partnership for CO_2 Sequestration (SWP). Hydrocarbons have been produced from the unit since 1956 and yielded 39,613,373 barrels (bbls) of oil and 28,979,870 MCF of natural gas as of February 28, 2015. Most of this production (36,342,520 bbls of oil) occurred as of November 30, 1986 (Munson, 1989). Since then an additional 1,819,254 bbls of oil were produced until the start of CO_2 flooding on November 30, 2010. CO_2 flooding carried out through February 28, 2015 has produced another 1,451,599 bbls of oil. Since 1986, only about 200,000 MCF of gas have been produced. Chaparral Energy has operated the Farnsworth Unit since December, 2009 and the Southwest Partnership began work there in April, 2013.

CO_2 may be sequestered in the subsurface by structural, capillary, solubility, and mineral trapping (IPCC, 2005). The focus of the present paper is on CO_2 sequestration through mineral trapping as a result of reaction of CO_2 with Morrow B formation water and reaction of the resultant CO_2-charged formation water with the Morrow B rock matrix. Mineral trapping is a particularly favorable form of CO_2 sequestration because of its potential for stable, long-term CO_2 sequestration by forming carbonate minerals (Gunter et al 1997, Oelkers et al., 2008). However, mineral precipitation and possibly dissolution

may also be important on shorter time scales as they may alter the porosity and permeability of the reservoir and thus the migration of fluids during injection. Thus, predicting how CO_2 injection will change the Morrow B pore water composition, mineralogy, porosity, and permeability are important components of evaluating the feasibility of large-scale CO_2 sequestration in the Morrow B at Farnsworth.

The Farnsworth Unit lies within the Anadarko basin, which has been well studied, so that the broad geologic context of the Farnsworth Unit is well understood. However, little direct work on the Farnsworth Unit has so far been published. Previous work includes publications by Parker (1956), Munson (1989), McKay and Noah (1996), and Ampomah et al. (2015), and unpublished masters' theses by Munson (1988) and Gallagher (2014) on the deposition, mineralogy, diagenesis, reservoir properties, and production history of the Morrow B Sandstone.

The current manuscript presents the results of equilibrium geochemical speciation and reaction path modeling for CO_2 injected into the Morrow B Sandstone in the Farnsworth Unit. The study sought to answer the following questions: (1) How will the composition of the Morrow B pore water and rock matrix change as a result of CO_2 injection? (2) How much CO_2 could be expected to be sequestered by mineral trapping? (3) How much would the hydraulic properties of the Morrow B Sandstone be likely to be altered by CO_2 injection?

Geologic background

The Farnsworth Unit is located in the western part of the Anadarko basin (Fig. 1), historically one of the most important hydrocarbon-producing regions in the USA. The

Morrow Sandstone, which is the focus of the present study, was deposited during the third main stage of Anadarko basin evolution, in which Pennsylvanian orogeny led to uplift of the Wichita-Amarillo block on the basin's southern margin and downwarping within the basin, allowing the accumulation of about 5500 m of mostly marine sediments (Johnson, 1989). Epeirogenic sediment deposition has characterized the subsequent fourth stage of basin evolution, which is preserved mainly as about 2000 m of Permian red beds and evaporites. The first two stages of basin evolution consisted of Early to Middle Cambrian emplacement of igneous rocks upon 1300 to 1600 Ma basement rock, followed by Late Cambrian through Mississippian deposition of about 4500 m of sediments consisting mainly of carbonates and lesser amounts of fine- to medium-grained clastics.

In the Farnsworth Unit, the Morrow Sandstone has an average thickness of about 275 m and has been subdivided into a lower, middle, and upper section (Munson, 1989; Fig. 2). The Lower Morrow consists of a transgressive series of shallow marine claystones, sandstones, and limestones that unconformably overlie Mississippian Chester Group sediments. The Middle Morrow consists mainly of carbonate and shale with minor sandstone. The Upper Morrow consists of about 115 to 150 m of mainly shales containing lenticular, discontinuous coarse-grained sandstones, reflecting a fluvial deltaic environment that prograded toward the southeast (Swanson, 1979).

Most of the hydrocarbon production from the Farnsworth field has come from the Morrow B Sandstone, and is where CO_2 is being injected in the present project as part of an enhanced oil recovery (EOR) effort. The Morrow B lies at a depth of about 2400 m at a temperature of 75° C with an initial reservoir pressure reported at 15.2 MPa, conditions under which CO_2 should exist in a supercritical state for increased storage efficiency

(Munson, 1989, Bergman & Winter 1995, Bergman & Winter 1997, Bachu 2002). Porosity in the Morrow B varies mainly from about 10-18% with an average of 14.5%, and permeability ranges from about 1 to 250 millidarcies (mD), with an average of 48 mD (Munson, 1989; Ampomah et al., 2015). Both porosity and permeability tend to be higher in the western than in the eastern part of the Farnsworth Unit. The thickness of the Morrow B Sandstone averages 9 m with a maximum of about 16 m. The Morrow B consists mainly of quartz, with minor plagioclase feldspar and clay minerals, and traces of calcite, siderite, ankerite, and dolomite. The clay minerals consist mainly of kaolinite and chlorite, with minor illite and traces of smectite. The initial water saturation in the Morrow B at the time of the discovery of the Farnsworth Unit was 31.4% (Ampomah et al., 2015) and the Morrow B remains water wet, allowing ample opportunity for water-rock chemical reactions.

Conformably overlying the Upper Morrow is the Thirteen Finger Limestone, the lowest member of the Pennsylvanian Atoka Series, and an aquitard. The base of the Thirteen Finger consists of a thin coal bed overlain by finely crystalline dolomitic limestones and shales.

Methodology

All geochemical speciation and reaction path modeling calculations were based on Morrow B Sandstone pore water samples collected from well batteries, AWT#3 and AWT#4, on September 24, 2012, January 15, 2013, and April 11, 2013. Water samples were collected in one liter wide-mouth high density polyethylene bottles. To ensure that clean and representative pore water samples were collected, water lines were thoroughly

flushed before sampling. After collection, water samples were immediately placed in a cooler, then within two days upon returning to the laboratory were filtered through a 0.22 μm syringe filter to remove oil and dirt. Filtered water samples were typically analyzed for chemical composition within 1-2 weeks of collection in the field.

The pH and oxidation-reduction potential (ORP) of water samples were measured using a Thermo Fisher Dual Star Benchtop pH/ISE meter, an Orion 8102BNUWP glass combination pH electrode, and an Orion 9179BN Triode Low Maintenance ORP electrode. Water conductivity was measured using an Orion Model 162A conductivity meter and an Orion 01801A conductivity cell. Water alkalinity was measured with electrometric titration following the American Society for Testing and Materials (ASTM) D1067-02 method. The concentrations of major cations, Li^+, Na^+, K^+, Mg^{2+}, and Ca^{2+}, and major anions, F^-, Cl^-, Br^-, NO_3^{2-},and SO_4^{2-} were determined by ion chromatography using a Dionex DX-120 equipped with an IonPac CS-12A column for cation analysis and an IonPac AS9-HC column for anion analysis, following ASTM methods D6910-03 and D4327. Water samples were sent to the New Mexico Bureau of Geology and Mineral Resources to determine trace metal concentrations using inductively coupled mass spectrometry following U.S. Environmental Protection Agency (EPA) Method 200.8.

The time-averaged compositions of pore water from each well used in the modeling are shown in Table 1. In addition, aluminum and iron concentrations were obtained by assuming saturation with respect to illite and hematite, respectively. The relative mineral abundances and porosity of the Morrow B used in the reaction path modeling were based on the analyses of Munson (1989) and Gallagher (2014), and are shown in Table 2. Calculations were carried out at the reservoir temperature of 75° C.

All of the chemical modeling calculations were carried out using the Geochemist's Workbench® software and the *thermo.com.v8.r6+* thermodynamic database for pressures and temperatures on the liquid-vapor saturation curve for water. The resultant model fluid pressure of 0.039 MPa at 75° C is significantly lower than the actual reservoir pressure of 15.2 MPa. Reactions that are likely to be most sensitive to this pressure discrepancy involve gas species, so for the present study, the equilibrium constant for the CO_2 gas formation reaction in the *thermo.com.v8.r6+* database was replaced with the value for 15.2 MPa and 75° C, calculated using the SUPCRT92b software (Johnson et al., 1992). The difference in log K value at water-saturation versus reservoir pressure at 75° C was small. In this simulation, the modified log K value of −8.769 was used instead of original log K value of −8.776.

Speciation calculations were first carried out to learn what minerals should be expected to precipitate or dissolve given the current composition of the Morrow B pore fluid prior to the scheduled CO_2 injection. Reaction path modeling was then done to explore the effects of CO_2 on the composition of the Morrow B pore fluid and to determine how the CO_2-charged pore fluid would react with the host rock. Reaction path modeling was done in two stages. In the first stage, CO_2 was gradually added to Morrow B Sandstone pore water up to its solubility limit of 46 g/kg water at 75° C, 15 MPa, and a salinity of 1M NaCl (Duan and Sun, 2003). The resultant CO_2-saturated pore water was then allowed to react with the Morrow B host rock mineralogy shown in Table 2.

Two scenarios were considered for the second stage of the reaction path modeling—one in which the pore fluid was allowed to react with enough rock to create a 1% increase in porosity if all of that rock dissolved (i.e. a 100:1 water:rock ratio), and a

second in which the pore fluid was allowed to react with enough rock to create a 10% increase in porosity if all of that rock dissolved (i.e. a 10:1 water:rock ratio). This led to masses of reactant rock of 27 and 270 g, respectively per kg of water for a porosity of 14.5% and a bulk rock density of 2700 kg/m^3. The actual change in porosity that resulted in the two model scenarios differed from 1 and 10% because much of the dissolved rock reprecipitated but not necessarily as the same minerals that were dissolved, or as different minerals but with similar densities as those of the minerals that were dissolved.

All of the reaction path models were calculated assuming chemical equilibrium. The results that are presented therefore represent the maximum extent of chemical reaction possible, while also showing the evolution of fluid chemistry and host rock mineralogy en route to this maximum. Thus, although the results of the present study do not convey the time scale over which mineral sequestration would take place in the Farnsworth unit, they place a limit on how much mineral sequestration can be expected and serve as a useful benchmark for future studies that will employ reaction kinetics and transient fluid flow and solute transport.

Results

Speciation Modeling

Current Morrow B Sandstone groundwater is relatively dilute given its depth of about 2400 m, with a total dissolved solids (TDS) content of about 3600 mg/L, dominated by Na, Cl, bicarbonate, and Ca. Geochemical speciation modeling was carried out at an ORP (Eh) value of 140 mV and a pH of 7 for fluid compositions from both well batteries, AWT3 and AWT4, based on the averages of the water samples collected (Table 1). The

results showed the Morrow B formation water to be supersaturated mainly with respect to zeolite minerals (stilbite, mesolite, scolecite), clay minerals (saponite, montmorillonite, nontronite, kaolinite, beidellite), carbonate minerals (witherite, dolomite, strontianite, calcite, aragonite), mica minerals (muscovite, paragonite, celadonite), and aluminum hydroxides (diaspore, boehmite) (Fig. 3). The predicted zeolite-smectite-rich mineral assemblage is typical of burial diagenetic environments (Hay, 1986), and clay minerals were reported by Munson (1989) and Gallagher (2014) to be present in the Morrow B Sandstone. The clay minerals are likely to be alteration products of feldspars, as K-feldspar, albite, and anorthite were all predicted to be undersaturated in the Morrow B pore fluid (Fig. 4). In contrast, quartz was predicted to be close to saturation, consistent with the quartz-rich nature of the Morrow B Sandstone.

Reaction path modeling: Stage 1

In the first stage of the reaction path modeling, CO_2 was progressively titrated into 1 kg of Morrow B pore water up to the solubility limit of CO_2 of 46 g/kg under reservoir conditions (Duan and Sun, 2003). Calculations were carried out for initial fluid compositions corresponding to Morrow B pore water sampled from both well batteries, AWT3 and AWT4, as shown in Table 1. The progressive addition of CO_2 caused a corresponding decrease in pH from 7.0 to a minimum of 4.1 and 4.2 in the AWT3 and AWT4 model pore fluids, respectively, at CO_2 saturation (Fig. 5). In the reaction path models, the initial state of the system (at reaction progress variable, $\xi = 0$) was reset by lowering the pH to about 6.75 and the carbonate alkalinity by about 13 to 16% for model fluids AWT3 and AWT4, respectively, so that no supersaturated minerals existed. In the resulting modified initial state, strontianite, quartz, dolomite, and witherite were at

saturation for model fluid AWT4, and these minerals plus nontronite and mesolite were at saturation for model fluid AWT3.

Very few further changes in mineralogy were predicted as more CO_2 was titrated into the pore fluids (Fig. 6). The abundance of quartz remained constant at about 2×10^{-4} moles/kg water for both model fluids as CO_2 was added. Minerals that were produced in the initial state equilibration—dolomite, strontianite, mesolite, and Ca-nontronite in model fluid AWT3, and strontianite in model fluid AWT4—completely dissolved away with the first pH decrease and therefore do not appear in Figure 6. For model fluid AWT4, dolomite persisted until pH had decreased to 6.13 at a ξ value of only 0.01. Diaspore was predicted to precipitate early in the reaction path for both wells. For model fluid AWT3, diaspore abundance remained relatively constant at about 5×10^{-5} moles/kg water, whereas for AWT4, diaspore reached a maximum abundance of about 4×10^{-8} moles/kg water at ξ = 0.1, decreasing thereafter until its disappearance after $\xi = 0.6$. Witherite declined steadily in abundance over the reaction path for both model fluids from a maximum of about 10^{-5}, disappearing by $\xi = 0.1$ for model fluid AWT3 and by $\xi = 0.27$ for model fluid AWT4.

Reaction path modeling: Stage 2

In the second stage of reaction path modeling, CO_2 charged fluid was allowed to react with Morrow B host rock in volumetric water:rock ratios of 100:1 and 10:1. The initial pH and CO_2 fugacity were taken from the results of the stage one reaction path model at CO_2 saturation. The initial pH value was 4.1 for the AWT3 fluid and 4.2 for the AWT4 fluid. The initial CO_2 fugacity for both fluids was 7.8 MPa.

Figure 7 shows the pH as a function of reaction progress for model fluids AWT3 and AWT4 for volumetric water:rock ratios of 100:1 and 10:1. The results for the two model fluids are similar, but pH rose to a slightly higher level of 5.1 to 5.2 for the lower water:rock ratio case compared to about 4.7 for the higher water:rock ratio case. The increase in pH is due to the consumption of minerals like calcite and albite, which react with H^+ to form bicarbonate and clay and aluminum hydroxide alteration minerals like nontronite and diaspore (Fig. 8). Because more rock is available for reaction in the lower water:rock ratio scenario, the pH can be buffered to a higher value.

Diaspore was predicted to be the principal alteration mineral formed in all of the reaction path models, accounting for up to 0.22 mol/kg water by the end of the AWT3 reaction path model for a 10:1 water:rock ratio (Fig. 8c). Mg-nontronite, in contrast, was predicted to be orders of magnitude less abundant than diaspore. Siderite was the only other alteration mineral consistently predicted to form, precipitating in trace amounts up to about 10^{-3} mol/kg water for 100:1 water:rock ratio and 10^{-2} mol/kg for 10:1 water:rock ratio. Witherite was predicted to precipitate in model fluid AWT3 for a water:rock ratio of 10:1, and in model fluid AWT4 fluid for both water:rock ratios, reaching a maximum concentration of about 10^{-5} mol/kg water. Moderate amounts of dolomite and magnesite—up to about 0.04 mole/kg water—were predicted to precipitate in both model fluids at a water:rock ratio of 10:1, with magnesite precipitation beginning significantly later than dolomite precipitation.

Several reactant minerals consistently reprecipitated as products. The most important of these is quartz, which remained saturated throughout all of the simulations. The final amount of quartz precipitated was slightly larger than the amount of reactant

quartz, because some quartz formed through the dissolution of other reactant silicate minerals. After a period of dissolution, siderite reprecipitated after enough rock had reacted with the water to raise the pH to around 4.5.

Changes in aqueous elemental concentrations as a function of progressive reaction with the Morrow B host rock are shown in Figure 9. During high water:rock ratios, total aqueous concentrations of Na, Mg, K, and Ca increased due to dissolution of albite, calcite, chlorite, montmorillonite, and illite. Increasing reaction with rock led to eventual decreases in the aqueous concentrations first of Ca and then of Mg as dolomite began precipitating and then magnesite began reprecipitating. The concentration of aqueous SiO_2 remained constant because quartz remained saturated throughout all of the simulations. The total carbon concentration in both model fluids remained effectively constant for the high water:rock ratio scenario, indicating that carbonate mineral dissolution was balanced by carbonate mineral precipitation (Fig. 10). With increased rock reaction, carbonate mineral precipitation exceeded carbonate mineral dissolution, resulting in an approximately 0.02 mol/kg decrease in total carbon concentration in both model fluids by the end of the low water:rock ratio scenarios (Fig. 10). The aqueous concentration of Al in all simulations decreased progressively due to the precipitation of the Al-bearing minerals, diaspore and nontronite. The aqueous concentration of Ba held constant during high water:rock ratios, but as the amount of reaction with host rock increased, Ba concentration in the model fluids began to decrease with the onset of witherite precipitation.

All of the simulations showed net dissolution of the host rock. For the 100:1 water:rock simulations, the volume of the host rock decreased by 3.55% for model fluid AWT3 and by 3.51% for model fluid AWT4, which means that porosity would have

increased by the same amounts. For the 10:1 water:rock simulations, porosity increases were smaller at 1.51% for model fluid AWT3 and 1.37% for model fluid ATW4.

Discussion

The results of the present study suggest that the Morrow B Sandstone would be a geochemically favorable target for CO_2 sequestration. The predominance of quartz in the sandstone and the low salinity of the pore fluid combine to make the system resistant to major mineralogical changes. The Morrow B is predicted to remain composed predominantly of quartz, with the abundance of quartz increasing by about 10% from the initial abundance in all simulations. The growth in quartz abundance comes at the expense of silicate accessory minerals, mainly albite, which is converted to diaspore and nontronite. However, diaspore, the second most abundant mineral formed in the reaction path simulations, is more than an order of magnitude less abundant than quartz.

Uncertainty in the water:rock ratio of reaction leads to significant uncertainty in the results. However, as CO_2-charged water were to migrate further through the Morrow B from the injection well, the water would progressively react with more rock, such that the low water:rock scenario probably more closely represents long-term conditions. Thus, the long-term change in porosity, especially farther from the injection well, is likely to be closer to the 1.37 – 1.51% range predicted in the 10:1 water:rock ratio scenario than to the 3.51 to 3.55% range predicted by the 100:1 water:rock ratio scenario. In addition, the pH of the CO_2-charged fluid is more likely to be buffered to a value above 5 than below 5, allowing more carbonate mineral precipitation and a net decrease in dissolved carbon concentration rather than a net increase (Fig. 10). However, the low TDS content of the

Morrow B formation water and low abundance of minerals in the Morrow B that contain cations readily capable of forming carbonate minerals means that the total amount of carbonate mineral precipitation is low—about 0.3% of the total rock volume for the 100:1 water:rock ratio case and about 2.3 to 2.4% of the total rock for the 10:1 water:rock ratio case. Thus, a maximum of only about 2% of the 46 g of CO_2 per kg water at CO_2 saturation is consumed to form carbonate minerals in the model scenarios investigated. This means that much more CO_2 would be expected to be sequestered by solubility trapping than by mineral trapping.

Numerous additional factors not considered in the present study could affect the fate of CO_2 injected into the Buckhaults Sandstone, including dissolution into hydrocarbon phases, reaction kinetics, and the advective transport of CO_2 both as a separate immiscible phase and as a solute in the hydrocarbon and aqueous phases, and dispersion. Most of these factors would reduce the concentration of CO_2 in the Buckhaults formation water and the progress of carbonate mineral formation reactions. The reaction path models also force the dissolution of minerals beyond their solubility. Some minerals, like quartz, then simply reprecipitate at the next reaction step, but other minerals remain dissolved and their constituents precipitate as different minerals at the next reaction step. Thus, the reaction path models in the present study probably predict well the sequence of mineral precipitation, dissolution, and fluid composition changes caused by CO_2 injection into the Morrow B formation water, but over predict the changes in mineral abundances and porosity.

Conclusions

Despite significant uncertainties in the models, some conclusions can be drawn. Speciation calculations showed the Morrow B pre-CO_2-injection formation water to be supersaturated with respect to an assemblage of zeolite, clay, carbonate, mica, and aluminum hydroxide minerals, and quartz. This assemblage is consistent with a burial diagenetic environment and the quartz-rich nature of the Morrow B in which the principal accessory minerals, the feldspars and chlorite, are predicted to dissolve and are observed petrograpically to be undergoing alteration (Munson, 1989; Gallagher, 2014). Titration of CO_2 into the Morrow B formation water to the point of saturation given its current pressure, temperature, and salinity lowered the pH to around 4.1 to 4.2. Quartz was predicted to precipitate throughout the titration and diaspore and witherite precipitated more variably.

Reaction of the CO_2-charged formation water with the Morrow B host rock caused the pH to recover to a final value of about 4.6 to 4.7 for the 100:1 water:rock ratio scenario, and to a final value of 5.1 to 5.2 for the 10:1 water:rock ratio scenario. Diaspore and Mg-nontronite were predicted to precipitate throughout reaction of the CO_2-charged water with the Morrow B host rock. The carbonate minerals, siderite, witherite, dolomite, and magnesite, formed respectively as the pH of the fluid rose. The final amount of precipitated quartz was slightly higher than the amount of reactant quartz because of silica released into solution by alteration of minerals like albite to diaspore and Mg-nontronite. The concentrations of Na, Mg, K, and Ca initially increased as albite, calcite, chlorite, montmorillonite, and illite dissolved, but then Ca and Mg concentrations decreased as dolomite and magnesite began to precipitate. The maintenance of quartz saturation

throughout the reaction paths caused silica concentration to remain constant. However, Al and Ba concentrations decreased due to diaspore, nontronite, and witherite precipitation.

Mineral trapping would only be a sink for CO_2 at relatively low water:rock ratios, consuming about 2% of the 46 g/kg CO_2 at saturation concentration. At high water:rock ratios, carbonate mineral precipitation is essentially balanced by carbonate mineral dissolution. The overall porosity change at the low model water:rock ratio of 10:1 was on the order of about 1.4 to 1.5%. Thus, the hydraulic properties of the Buckhaults Sandstone should not be greatly altered by chemical reactions associated with CO_2 injection.

References

Ampomah, W., R. S. Balch, and R. B. Grigg, 2015, Analysis of Upscaling Algorithms in Heterogeneous Reservoirs with Different Recovery Processes, SPE – 173588 – MS, SPE Production Operations Symposium, Oklahoma City, Oklahoma, USA.

Bergman, P. D. and E. M. Winter, 1995, Disposal of carbon dioxide in aquifers in the U.S.: Energy conversion and management, v. 36, no. 6 – 9, p. 523 – 526.

Bergman, P. D., E. M. Winter, and Z. Y. Chen, 1997, Disposal of power plant CO_2 in depleted oil and gas reservoirs in Texas: Energy conversion and management, v. 38, p. S211 – S 216.

Bachu S., 2002, Sequestration of CO_2 in geological media in response to climate change: roadmap for site selection using the transform of the geological space into the CO_2-phase space: Energy Convers Manage, v. 43, p. 87–102.

Dai. Z., R. Middleton, H. Viswanathan, J. F. Rahn, J. Bauman, R. Pawar, S. Y. Lee, B. McPherson, 2014, An Integrated Framework for Optimizing CO2 Sequestration and Enhanced Oil Recovery: Environmental Science and Technology Letters, v. 1, p. 49 – 54.

Duan, Z., and R. Sun, 2003, An improved model calculating CO_2 solubility in pure water and aqueous NaCl solutions from 273 to 533 K and from 0 to 2000 bar: Chemical Geology, v. 193, p. 257 – 271.

Gallagher, S. R., 2014, Depositional and diagenetic controls on reservoir heterogeneity: Upper Morrow Sandstone, Farnsworth Unit, Ochiltree County, Texas: Master's Thesis, New Mexico Institute of Mining and technology, Socorro, New Mexico, p. 215.

Gunter, W. D., B. Wiwchar, and E. H. Perkins, 1997, Aquifer disposal of CO_2 – rich greenhouse gases: extension of the time scale of experiment for CO_2 – sequestering reactions by geochemical modeling: Mineralogy and Petrology, v. 59, p. 121 – 140.

IPCC, 2005, IPCC special report on carbon dioxide capture and storage, prepared by Working Group III of the Intergovernmental Panel on Climate Change: Cambridge, United Kingdom and New York, NY, USA, Cambridge University Press, p. 442.

Johnson, K. S.; Amsden, T. W.; Denison, R. E.; Dutton, S. P.; Goldstein, A. G.; Rascoe, B., Jr.; Sutherland, P. K.; and Thompson, D. M., 1988, Southern Mid - continent region, in Sloss, L. L. (ed.), Sedimentary cover-North American craton, U.S.: The Geology of North America, Geological Society of America, Boulder, v. D-2, p. 307-359.

Johnson, K, S., 1989, Geologic evolution of the Anadarko Basin: Oklahoma Geological Survey Circular, v. 90, p. 3 – 12.

Johnson, J. W., E. H. Oelkers, and H. C. Helgeson, 1992, SUPCRT92: A software package for calculating the standard molal thermodynamic properties of minerals, gases, aqueous species, and reactions from 1 to 5000 bar and 0 to 1000°C: Computer and Geosciences, v. 18, no. 7, p. 899 – 947.

McKay, R. H., and J. T. Noah, 1996, Integrated perspective of the depositional environment and reservoir geometry, characterization, and performance of the Upper Morrow Buckhaults Sandstone in the Farnsworth Unit, Ochiltree County, Texas: Oklahoma Geological Survey Circular, v. 98, p. 101-114

Munson, T. W., 1988, Depositional, diagenetic, and production history of the Upper Morrowan Buckhaults Sandstone, Farnsworth Field, Ochiltree County Texas: Master's Thesis, West Texas University, Canyon, Texas, p. 117.

Munson, T,W., 1989, Depositional, diagenetic, and production history of the Upper Morrowan Buckhaults Sandstone, Farnsworth Field, Ochiltree County Texas: Oklahoma City Geological Society, Shale shaker, v. 40, no.13, p. 2 – 20.

Oelkers E. H., S. R. Gislason, J. Matter, 2008, Mineral carbonation of CO_2: Elements, v. 4, p. 333-337.

Parker, R. L., 1956, "Farnsworth Morrow Oil Field": *The Panhandle Geonews*, v. 4, no. 1, p.5-12.

Swanson, D. C., 1979, Deltaic deposits in the Pennsylvanian upper Morrow Formation of the Anadarko basin, in Hyne, N. J. (ed.), Pennsylvanian sandstones of the Mid – Continent: Tulsa Geological Survey Special Publication, v. 1, p. 115 – 168.

White, M.D., B. J. McPherson, R.B. Grigg, W. Ampomah, and M. S. Appold, 2014, Numerical Simulation of Carbon Dioxide Injection in the Western Section of the Farnsworth Unit: Energy Procedia, v. 63, p. 7891 – 7912.

Figures

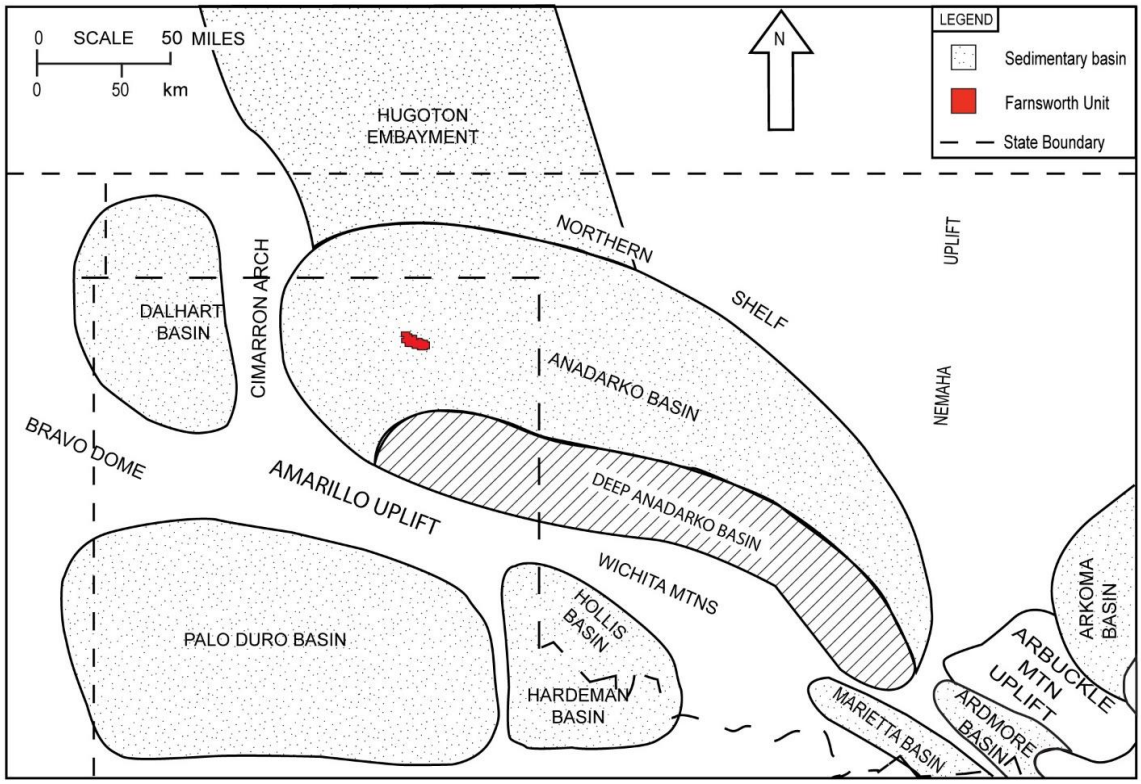

Figure 1: Geologic context and location of the Farnsworth Unit (modified after Johnson et al., 1988).

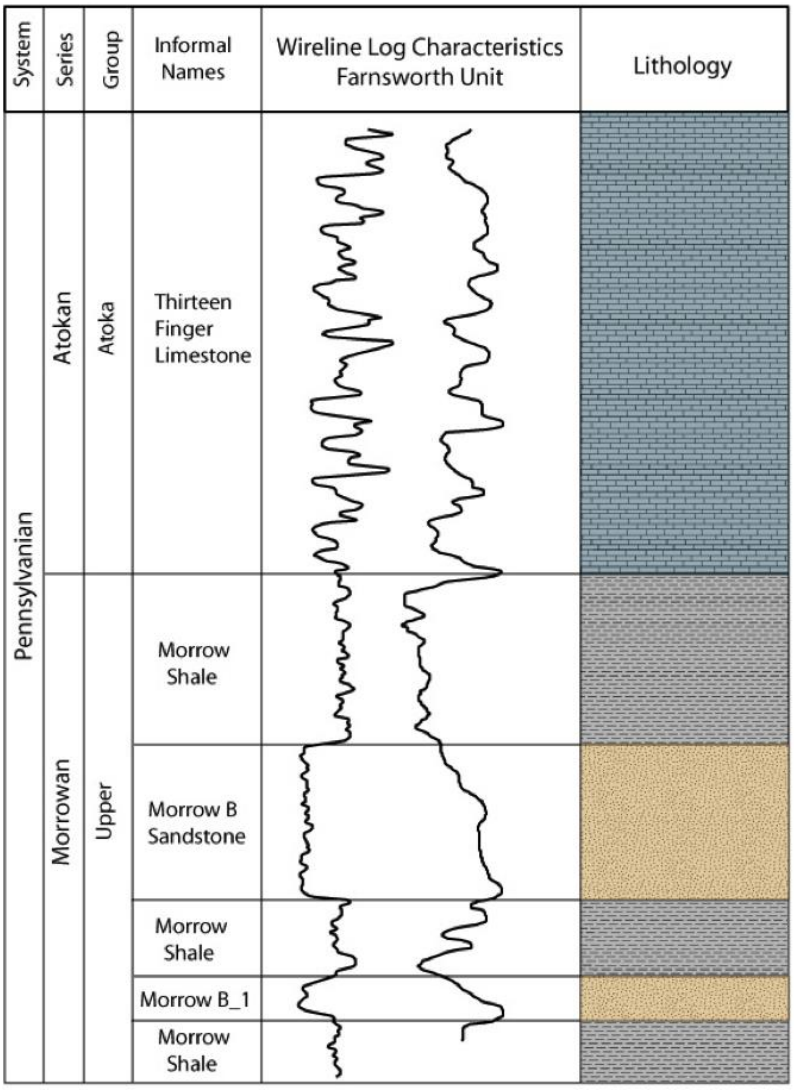

Figure 2: Stratigraphic chart showing divisions of the Upper Morrowan and Lower Atokan-aged strata in the Farnsworth Unit. Wireline log is from well 32-2. Modified from Munson (1989) and Puckette et al. (2008) by Gallagher (2014).

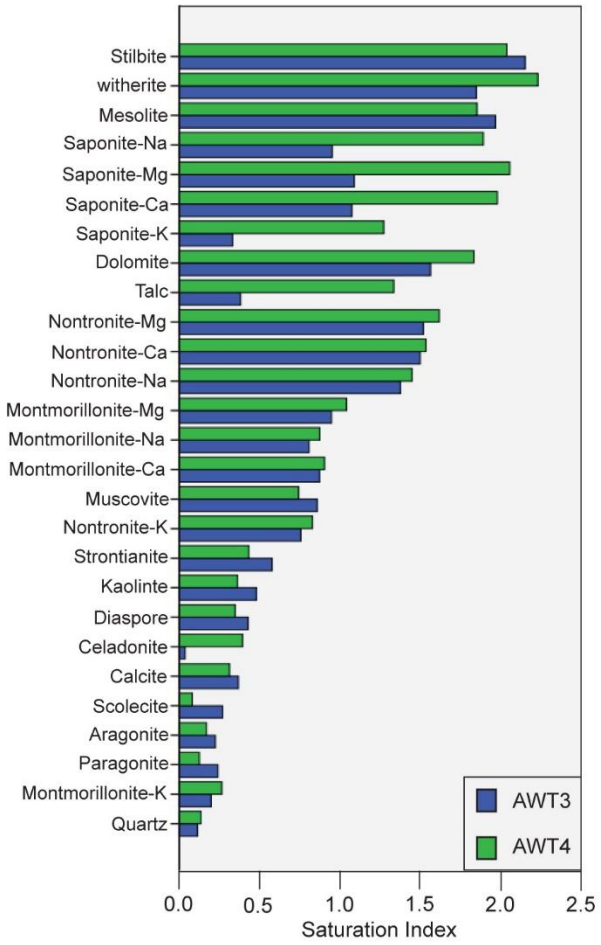

Figure 3: Minerals predicted to be supersaturated in Morrow B Sandstone formation water sampled from well batteries, AWT3 and AWT4.

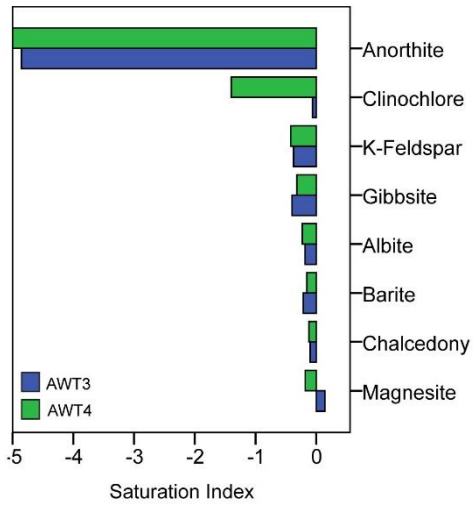

Figure 4: Minerals predicted to be undersaturated in Morrow B Sandstone formation water sampled from well batteries, AWT3 and AWT4.

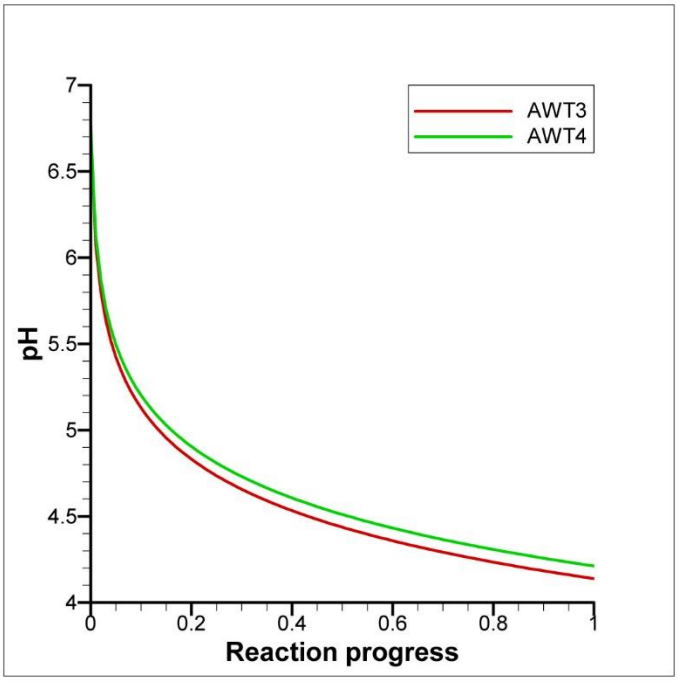

Figure 5: Predicted change in pH of Morrow B Sandstone formation water during stage 1 reaction path modeling

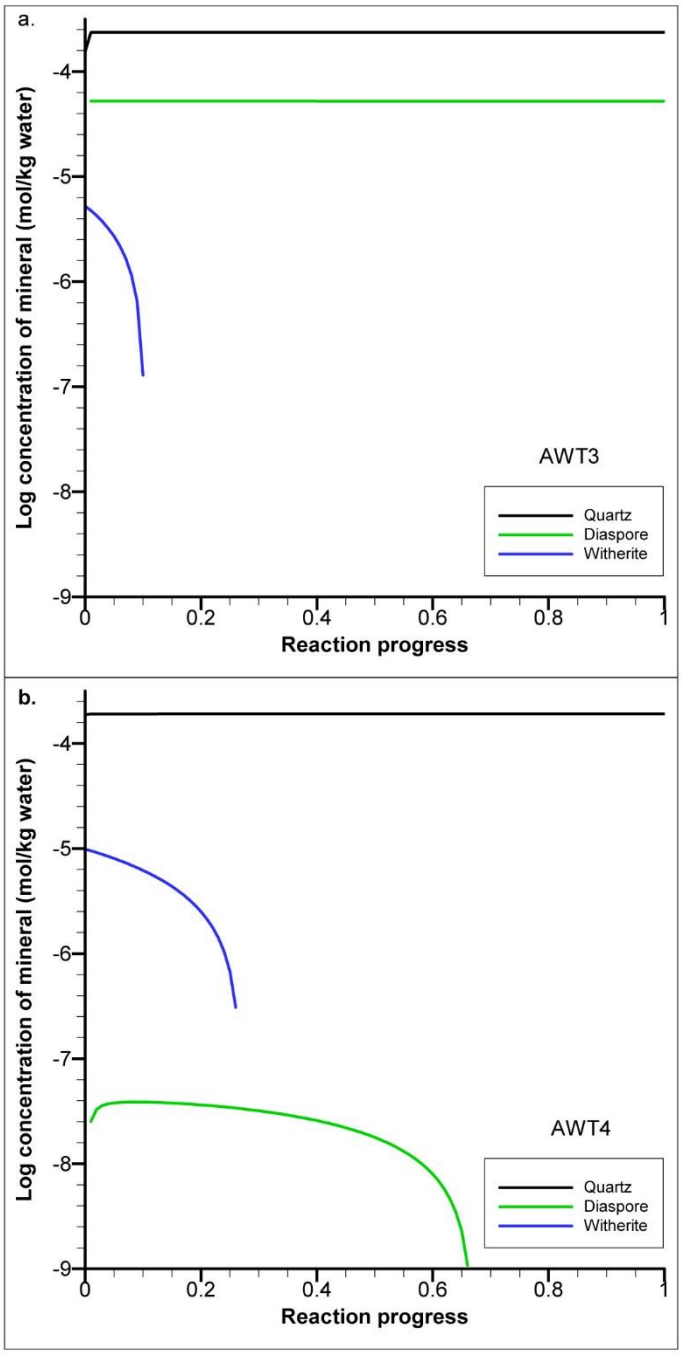

Figure 6: Predicted mineral precipitation during stage 1 reaction path modeling (a) model fluid AWT3 (b) model fluid AWT4.

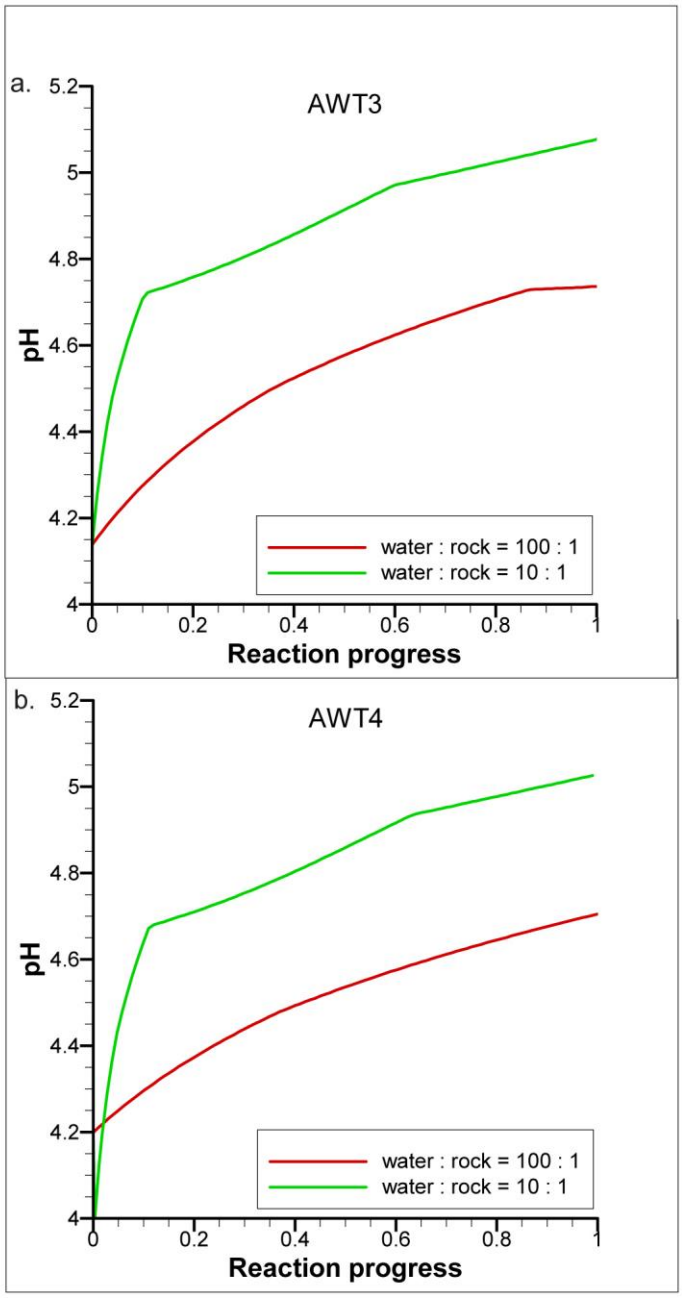

Figure 7: Predicted change in pH during stage 2 of the reaction path modeling for model fluids (a) AWT3 and (b) AWT4 for final water:rock ratios of 100:1 and 10:1.

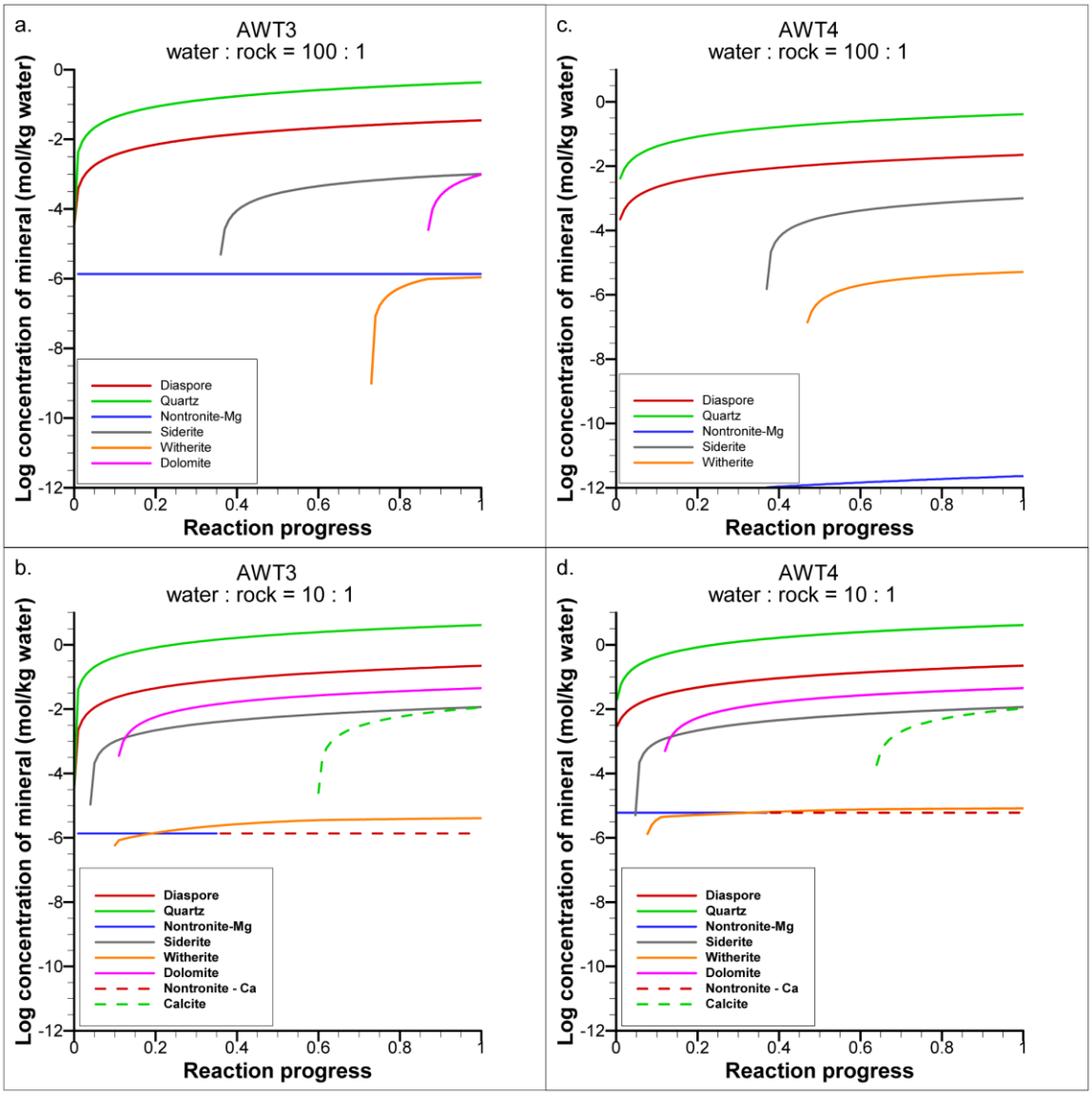

Figure 8: Predicted mineral precipitation for stage 2 of the reaction path modeling for (a) model fluid AWT3 and a final water:rock ratio of 100:1, (b) model fluid AWT3 and a final water:rock ratio of 10:1, (c) model fluid AWT4 and a final water:rock ratio of 100:1, (d) model fluid AWT4 and a final water:rock ratio of 10:1.

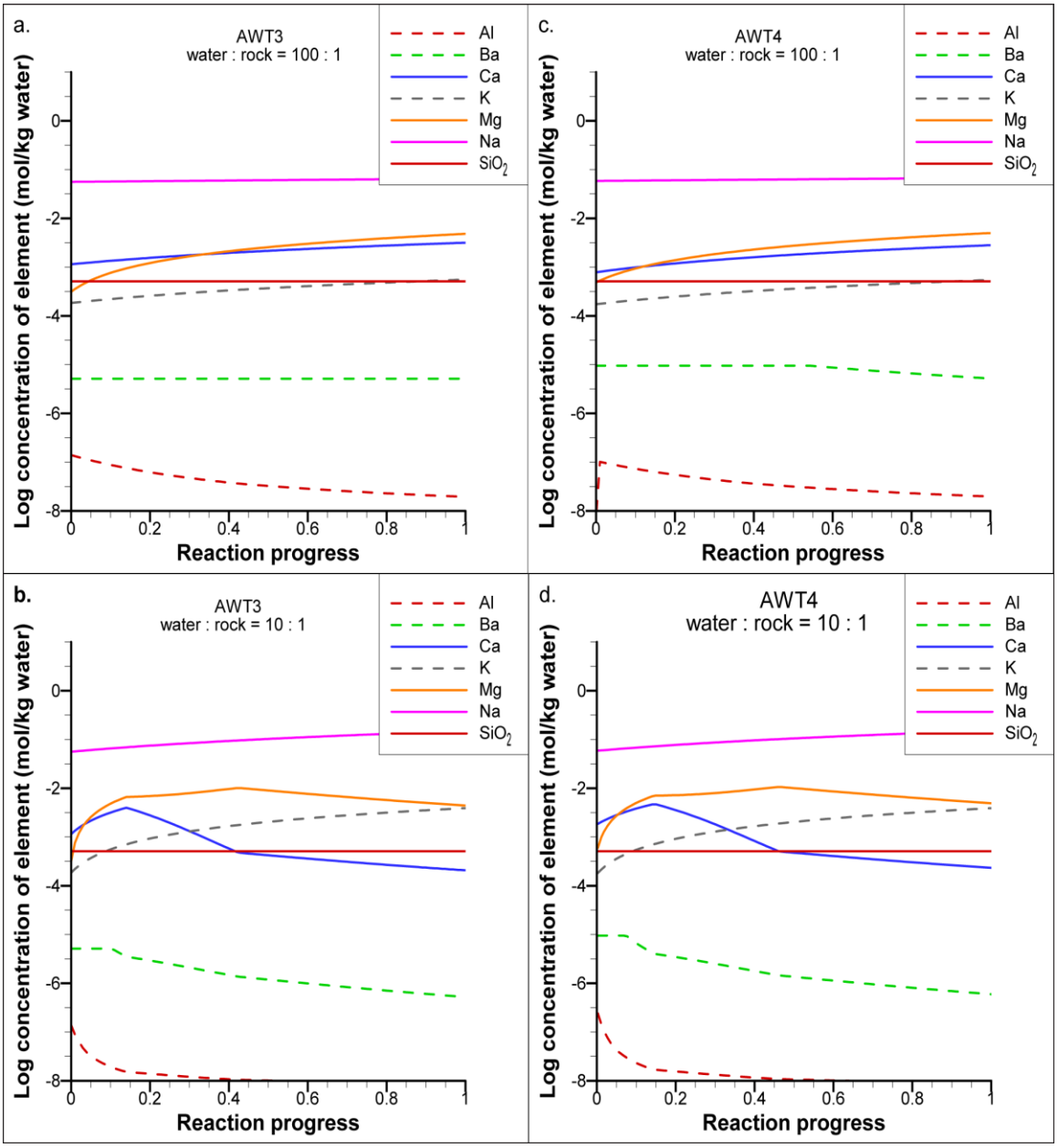

Figure 9: Predicted changes in total elemental concentration during stage 2 of the reaction path modeling for (a) model fluid AWT3 and a final water:rock ratio of 100:1, (b) model fluid AWT3 and a final water:rock ratio of 10:1, (c) model fluid AWT4 and a final water:rock ratio of 100:1, (d) model fluid AWT4 and a final water:rock ratio of 10:1.

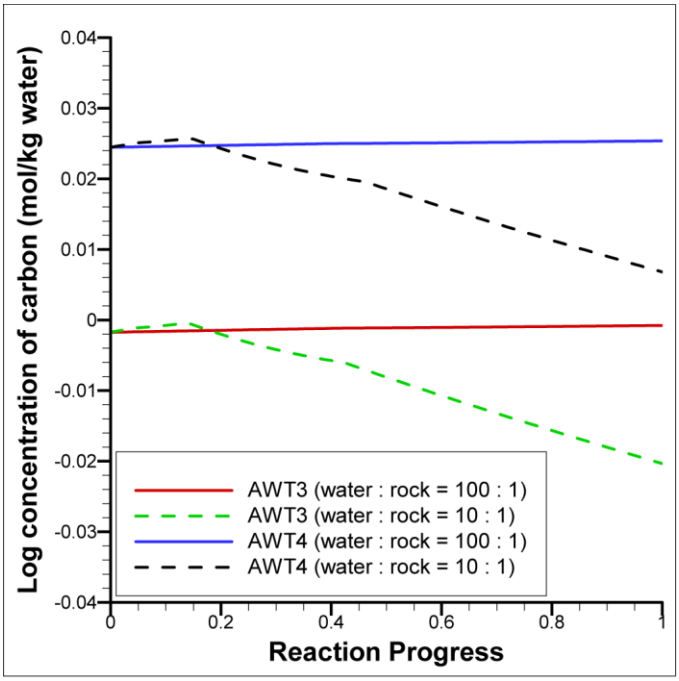

Figure 10: Predicted changes in the concentration of total dissolved carbon for stage 2 of the reaction path modeling for model fluids AWT3 and AWT4, and final water:rock ratios of 100:1 and 10:1.

Table 1: Composition of pore water sampled from well batteries, AWT3 and AWT4, and employed in the modeling.

Basis species	AWT3 mg/kg in fluid	AWT4 mg/kg in fluid
Al^{+++}	1.05	0.00791
$B(OH)_3(aq)$	21.5	27.8
Ba^{++}	0.592	1.37
Br^-	17.8	20.3
Ca^{++}	38.5	32.9
Cl^-	1.47E+03	1.84E+03
F^-	0.654	0.911
Fe^{++}	7.29E-05	2.10E-08
HCO_3^-	5.79E+04	795
K^+	7.87	7.11
Li^+	0.283	0.461
Mg^{++}	6.27	12.3
Na^+	1.08E+03	1.41E+03
SO_4^{2-}	21.4	12.9
SeO_3^{2-}	0.0687	0.0827
$SiO_2(aq)$	24.5	42.1
Sr^{++}	2.68	1.85
Zn^{++}	1.51E-05	0.108
pH	7	7
Eh (mV)	140	140

Table 2: Mineral composition of the Morrow B Sandstone employed in the modeling based on the average of petrographic characterizations by Munson (1989) and Gallagher (2014).

Minerals	**Volume (%)**
Quartz	84.26
Albite	9.0
Calcite	0.75
Ankerite	0.25
Siderite	0.25
Montmorillonite	0.1
Illite	0.88
Chlorite	1.79
Kaolinite	2.72

Part II

REACTIVE TRANSPORT MODELING OF CO_2-BRINE-ROCK INTERACTIONS IN THE FARNSWORTH, TEXAS HYDROCARBON UNIT, USA

Introduction

The purpose of the present study was to investigate the physical and chemical effects of CO_2 injection in the Farnsworth Hydrocarbon Unit in northern Texas, USA (Fig. 11). The study is part of a broader effort by the U.S. Department of Energy-sponsored Southwest Partnership on Carbon Sequestration and Chaparral Energy to evaluate the potential of the Farnsworth Unit for large-scale CO_2 sequestration while enhancing oil recovery. The main target for CO_2 injection is the Morrow B Sandstone, a formation in the Upper Morrowan (Early Pennsylvanian) Series of fluvial deltaic sediments and the principal hydrocarbon reservoir in the Farnsworth Unit. The Farnsworth Unit has produced 39,613,373 barrels of oil and 28,979,870 cubic feet of natural gas since its discovery in 1956. Chaparral Energy began producing hydrocarbons from the field in December, 2009.

The geology and hydrocarbon production history of the Farnsworth Unit has been documented in several previous studies, including Parker (1956), Munson (1988, 1989), McKay and Noah (1996), Gallagher (2014), and Ampomah et al. (2015). White et al. (2014) carried out a numerical modeling study simulating primary, secondary, and tertiary recovery of hydrocarbons from the Farnsworth Unit that incorporated the non-isothermal flow of CO_2, methane, brine, and multi-component petroleum. The first part of the present study used reaction path modeling to study the effects of CO_2 injection on the composition of the pore water and the mineralogy of the Morrow B Sandstone. The second part of the present study, presented here, reports the results of a reactive transport modeling study that simulated the injection of CO_2 into the Morrow B, the flow of CO_2 and the Morrow B formation water, the transport of solute in the formation water, and chemical reactions between CO_2, water, and the Morrow B mineral matrix. The study sought to address the

following specific questions: (i) How will fluid pressure change in the Morrow B reservoir due to CO_2 injection? (ii) How will CO_2 migrate through the reservoir and how much CO_2 will leave the reservoir? (iii) How will CO_2 be distributed among aqueous, immiscible gas, and mineral phases? (iv) How will porosity and permeability change as a function of mineral precipitation and dissolution? (v) How will pore water composition change as a result of CO_2 injection?

Geologic Background

The Farnsworth hydrocarbon unit covers about 115 km^2 in northern Texas, USA in the western Anadarko basin. The target reservoir for CO_2 injection and enhanced oil recovery in the Farnsworth Unit is the Morrow B Sandstone, previously called the Buckhaults Sandstone. The Morrow B is one of five channel sandstone units deposited in fluvial valleys incised into the shales of the Upper Morrowan series (Fig. 12). The Morrow B on average accounts for about 9 m of the overall 115 to 150 m of the Upper Morrowan series. The Morrow B on average consists of about 84% quartz, 9% plagioclase feldspar, 3% kaolinite, 2% chlorite, and less than 1% each of calcite, ankerite, siderite, montmorillonite, and illite (Table 4). The Morrow B lies at a depth of about 2300 to 2450 m, dipping to the southeast, at a temperature of about 75° C and an initial reservoir pressure of about 15.2 MPa. The porosity of the Morrow B varies mainly from about 10-18% and the permeability varies from about 1 to 250 millidarcies (mD). Hydrocarbons in the Morrow B are trapped stratigraphically by updip porosity pinchouts (McKay and Noah, 1996). The porosity and permeability of the Morrow B tend to be higher in the western part of the Farnsworth Unit compared to the eastern part, though the reasons for these differences have not yet been discovered (Gallagher, 2014). Conformably overlying the

Upper Morrowan Series is the Atokan age Thirteen Finger Limestone, which acts as a cap rock for the Upper Morrowan Series. Underlying the Upper Morrowan Series is the Middle Morrowan Series, which consists mainly of marine carbonates and shales and minor sandstone. The Lower Morrowan Series consists of marine transgressive package of claystones, sandstones, and limestones unconformably overlying Mississippian strata.

Model Set-up

Numerical reactive transport simulations were carried out over a three dimensional model domain consisting of the thickness of the Morrow B Sandstone and overlying Morrow Shale (Fig. 12) over the full plan view area of the Farnsworth Unit (Fig. 13). The thickness, porosity, and permeability variation of the Morrow B and Morrow Shale over the model domain were determined from well logs and geophysical surveys compiled by Ampomah et al. (2015) to form a geologic model grid with cell dimensions of 764×468×10. The geological model grid was then upscaled to a 110×80×7 grid using an arithmetic averaging algorithm in order to carry out the reactive transport modeling simulations. The resultant reactive transport modeling grid contained 35 discrete porosity-permeability divisions (Table 6), with little correlation between porosity and permeability. In this grid, the five lowermost cell layers were assigned to the Morrow B Sandstone and the two uppermost cell layers were assigned to the Morrow Shale.

Several further initial conditions were prescribed to the model. Fluid pressure was assigned a value of 15.2 MPa at the western boundary of the grid at the base of the Morrow B and allowed to decrease eastward according to a regional hydraulic head gradient of 2.2×10^{-3} (assumed to be equal to the regional topographic gradient), and to decrease

hydrostatically with increasing elevation. Thus, the resulting equation describing the initial fluid pressure distribution as a function of distance (x) eastward from the western boundary of the model domain and elevation (z) above sea level is

$$P = \rho g(134 - 2.2 \times 10^{-3}x - z) \qquad (1)$$

where P is fluid pressure (Pa), ρ is fluid density, and g is gravitational acceleration. The model domain was assumed to have an initially homogeneous temperature of 75° C and homogeneous formation water salinity of 3600 mg/kg. All porous media in the model were assumed to be initially fully saturated with water. The initial formation water composition is shown in Table 2 and is based on analyses for the Morrow B reported in Part 1 of this thesis. The initial mineral composition in the model is shown in Table 4 and was derived from petrographic analyses of the Morrow B reported in Munson (1989) and Gallagher (2014).

Several boundary conditions were prescribed in the model. The top and bottom boundaries of the grid were prescribed as no fluid flow boundary conditions open to solute transport. The lateral boundaries were open to both fluid flow and solute transport. Nine CO_2 injection wells with pumping schedules shown in Figure 14, and geographic coordinates, screen depth intervals, and fluid enthalpy shown in Table 5 were assigned to the western part of the grid.

Relative permeability was defined according to the van Genuchten-Mualem model (Pruess, 1999) using a residual water saturation of 0.15, a residual CO_2 saturation of 0.1 (White et al., 2014), and the Mualam model parameter of $\lambda = 0.457$ (Pruess & Garcia, 2001, Xu, et al., 2005). The relationship between capillary pressure and saturation was defined

according to a van Genuchten function (Pruesss, 1999) using an α (strength coefficient) value of 19.61 kPa typical of sandstone (Pruess & Garcia, 2001, Xu, et al., 2005) and a maximum pressure of 15.2 MPa. Based on the recommendation of Pruess and Garcia (2002), the residual water saturation was set to zero for capillary pressure calculations. This is to prevent capillary pressure from going to negative infinity in the van Genuchten model as the relative permeability for water approaches zero as water saturation approaches the residual water saturation.

Reactive transport simulations were executed using the TOUGHREACT computer program with the ECO2N equation of state for NaCl brine and CO_2 and the EQ3/EQ6 thermodynamic database (Xu et al., 2004). Kinetic parameters for the precipitation and dissolution of minerals were taken from the compilation of Palandri and Kharaka (2004) and surface areas were based on Xu et al., (2004). Changes in permeability as a function of changes in porosity caused by mineral precipitation and dissolution were calculated according to a "tube-in-series" model (Pruess, 2005) fit to observed porosity-permeability data for the Morrow B (Dai et al., 2013). The best fit for this model occurred for $\Gamma = 2$ and $\varphi_r = 0.75$, where Γ represents the fractional length of the pore bodies and φ_r represents the fraction of original porosity at which permeability is reduced to zero. The "tube-in-series" model was found to represent the field porosity-permeability correlation of Dai et al. (2013) well for porosity changes of less than 5%.

The mutual solubilities of water and CO_2 in one another were computed according to Spycher and Pruess (2005). The dependence of water density on CO_2 concentration was calculated according to García (2001). The enthalpies of brine and CO_2 were calculated according to Lorenz and Müller (2003) and Altunin (1975), respectively. In the

simulations, CO_2 was injected at the reservoir temperature for 10 years at the rates shown in Figure 14, followed by a twenty year post-injection period. Aqueous species and gaseous species diffusion coefficients were set to 1.0×10^{-9} m^2s^{-1} and 1.1×10^{-5} m^2s^{-1}, respectively. Pore compressibility was set to 1.0×10^{-10} Pa^{-1}, an average value for sandstone (Ingebritsen and Appold, 2012), and the tortuosity factor was calculated to be 0.525 based on the 14.5% average porosity of the Morrow B.

Results

Figure 15 shows fluid pressure in the Morrow B after 1 month, 10 years, and 30 years. Injection of CO_2 raised fluid pressure to a maximum of about 19.2 MPa near the wells, which is still well below lithostatic pressure (Fig. 16). By the end of the CO_2 injection period after 30 years, maximum fluid pressure had fallen to about 15 MPa and the elevated fluid pressures had diffused broadly over the eastern part of the Farnsworth Unit. By 20 years after the cessation of CO_2 injection, fluid pressures in the western part of the Farnsworth Unit had dissipated enough to be comparable to fluid pressures downdip in the eastern part of the unit.

Figure 17 shows CO_2 gas saturation after 1, 10, and 30 years. CO_2 gas saturations increased over time around each injection well, with individual plumes gradually coalescing into larger plumes with maximum saturations for the most part around 0.5. The immiscible CO_2 gas plumes are not strongly affected by the regional west-east pressure gradient and remain largely centered on the injection wells. In contrast, CO_2 dissolved in aqueous solution is more mobile and appears to begin exiting the Farnsworth Unit along its northwestern boundary by 30 years (Fig. 18).

Most of the primary minerals in the Morrow B Sandstone were predicted to dissolve over the course of the simulations. Some of this is due to disequilibrium between the Morrow B formation water and rock matrix apart from the effects of CO_2, as the speciation modeling in Part I showed most of the primary minerals to be unstable in the presence of the Morrow B formation water, with the aluminosilicate minerals undergoing alteration to clay minerals. The injection of CO_2 into the Morrow B formation water accelerates this dissolution process by lowering the pH through the formation of carbonic acid. This is evident from Figure 19, which shows changes in the volume fraction of albite over time. Albite was predicted to dissolve throughout the model domain, but the greatest amounts of dissolution are in the vicinity of the injection wells where CO_2 concentrations are the highest and pH is the lowest. However, the overall amounts of albite dissolution are small, with volume fraction reductions no greater than about 0.00136. Silica introduced into the formation water by the dissolution of albite led to the precipitation of small amounts of quartz, with maximum volume fraction increases of about 0.00064 after 30 years located near the injection wells. Kaolinite was predicted to precipitate throughout the model domain, with maximum increases in volume fraction registered near the injection wells at 0.00086. Illite was predicted to precipitate near the injection wells and to dissolve away from injection wells, with changes in volume fraction ranging from -1.52×10^{-7} to 4.36×10^{-7}.

No secondary carbonate minerals were predicted to precipitate during the simulations. The abundances of the primary carbonate minerals could increase or decrease in the simulations. Calcite and siderite dissolved in proportion to the dissolved CO_2 concentration, reaching maximum volume fraction decreases of 0.0007 and 0.00023,

respectively (Figs. 21 and 22). The only carbonate mineral predicted to precipitate in the simulations, and thus the only mineral sink for CO_2 was ankerite (Fig. 23). The maximum predicted increase in volume fraction was 0.0013, which occurred near the injection wells. Magnesite and dolomite, which were predicted to precipitate in the reaction path models in Part I, were not predicted to precipitate in the reactive transport simulations thus far, but may with increased simulation time. The precipitation of ankerite outweighed the dissolution of other carbonate minerals and thus led to a net precipitation of carbonate minerals (Fig. 24). Thus, some mineral trapping of CO_2 is expected, but on a relatively small scale over the simulation times considered thus far.

However, because the volume fractions of minerals that were precipitated or dissolved were so small (of order 10^{-3} or less), porosity and permeability were negligibly affected.

Discussion

Sequestration scenario

The present model simulated the injection of about 2.5 million tonnes of CO_2 over 10 years into the Morrow B Sandstone in the Farnsworth Unit. This is a rate similar to the rate of CO_2 generation from a small coal-burning electric power plant (U.S. Environmental Protection Agency, 2012). Most of the injected CO_2 takes the form of an immiscible gas phase that is localized by capillary trapping around the injection wells for at least the 30 years simulated thus far. Over time, immiscible CO_2 gas accumulated at the top of the Morrow B Sandstone at the contact with the overlying shales as a result of buoyancy, accounting for about 64% of the total injected CO_2. A relatively smaller amount of CO_2 dissolves into aqueous solution (about 27% of the total injected CO_2), where it is more

mobile and begins to leave the geographic area of the Farnsworth Unit within 30 years. The amount of mineral precipitation and dissolution is small but extends throughout the aqueous CO_2 plume and would also be expected to continue downstream of the Farnsworth Unit over time. Significant carbonate mineral precipitation occurs—about 2.25×10^{8} kg or about 9 % of the 2.5 million tonnes of CO_2 injected—is sequestered in carbonate minerals as ankerite. Over long time scales this amount would increase as long as the plume of CO_2 gas persisted and could continue to dissolve into aqueous solution and replenish CO_2 removed through carbonate mineral precipitation. Thus, the Morrow B Sandstone is capable of sequestering large amounts of injected CO_2 within the confines of the Farnsworth Unit, though aqueous CO_2 and carbonate mineral precipitation would also be introduced into the Morrow B outside of the Farnsworth Unit by groundwater advection.

Risk associated with CO_2 plume

A major concern about large-scale CO_2 injection into the subsurface is that it could escape suddenly to the surface. The most likely avenues for such escape would be abandoned and undocumented wellbores or fractures. No known fractures or faults connect the Morrow B Sandstone to the surface or rocks near the surface. Also, increases in fluid pressure caused by CO_2 injection are well below lithostatic pressures, though fracture (rock matrix failure) pressures can be much lower than lithostatic pressure and have not yet been quantified in the Farnsworth Unit. Apart from the existence of fracture or wellbore conduits to the surface, the effects of capillary trapping and the existence of multiple aquitards between the Morrow B Sandstone and land surface make it unlikely for CO_2 to reach the land surface through bulk porous media flow.

Limitations of the model

The present reactive transport model has several uncertainties and limitations that affect the interpretation of how CO_2 injected into the Morrow B Sandstone will behave. Although porosity and permeability have been rigorously characterized through a combination of geophysical surveys and laboratory and field measurements, uncertainty remains, particularly with respect to heterogeneity. Considerable uncertainty exists in kinetic model parameters, particularly for mineral surface areas (Liu, et al., 2011) as a result of heterogeneity in grain size and shape.

Perhaps the biggest limitation of the model thus far is that it only treats brine and CO_2, whereas it is known that considerable petroleum and natural gas also exist in the Farnsworth Unit. Inclusion of petroleum and natural gas will have significant effects on relative permeability and capillary pressure relationships, which will affect the transport of CO_2 both as an immiscible phase and as a solute. In particular, petroleum is known to be a strong solvent for CO_2, which would reduce the amount of CO_2 present as a separate immiscible phase and perhaps increase the mobility of CO_2 overall if the relative permeability of oil were comparable to that of water.

Conclusions

Despite important uncertainties, some conclusions about proposed CO_2 sequestration in the Farnsworth Unit can be made on the basis of the present numerical model. Pore fluid pressures in the field should increase modestly during CO_2 injection but should dissipate quickly after injection ceases and should never exceed the lithostatic pressure. The immiscible CO_2 migrates to the top of the Morrow B Sandstone due to

buoyancy, forming a bubble of high CO_2 saturations centered around the injection wells. After 10 years, CO_2 saturation reached 0.4 and increased to 0.5 after 30 years due to the continued ascent of CO_2 as a result of buoyancy. The simulations predicted net dissolution of minerals due to disequilibrium between the Morrow B Sandstone formation water and rock matrix, and from the effects of injected CO_2. Kaolinite, illite and quartz precipitated at the expense of albite and chlorite, which dissolved. The primary carbonate minerals, calcite and siderite, in the Morrow B Sandstone dissolved throughout the simulations. The only carbonate mineral predicted to precipitate in the simulations was ankerite, making it the only mineral sink for CO_2. However, over the 30 years of simulation time carried out thus far, significant CO_2 mineral trapping occurs overall. Insignificant change in mineral dissolution and precipitation leads to negligible alterations in porosity and permeability. However, over time, the amount of CO_2 trapped in mineral phases will increase, whereas the amount of CO_2 sequestered in solution or as an immiscible phase will decrease.

CO_2 present as an immiscible gas phase is sequestered stably around the injection wells by capillary trapping. CO_2 present in the aqueous phase can be transported beyond the boundaries of the Farnsworth Unit within 30 years. Although CO_2 is likely to leak laterally through the Morrow B Sandstone out of the Farnsworth Unit mainly through groundwater and possibly hydrocarbon advection, it is unlikely to leak vertically out of the Morrow B Sandstone unless it is able to take advantage of unknown wellbores or fractures.

References

Altunin V. V, 1975, Thermophysical properties of carbon dioxide (in Russia): Publishing House of Standards, Moscow.

Ampomah, W., R. S. Balch, and R. B. Grigg, 2015, Analysis of Upscaling Algorithms in Heterogeneous Reservoirs with Different Recovery Processes, SPE – 173588 – MS, SPE Production Operations Symposium, Oklahoma City, Oklahoma, USA.

Bachu S., 2002, Sequestration of CO_2 in geological media in response to climate change: roadmap for site selection using the transform of the geological space into the CO_2-phase space: Energy Convers Manage, v. 43, p. 87–102.

Dai. Z., R. Middleton, H. Viswanathan, J. F. Rahn, J. Bauman, R. Pawar, S. Y. Lee, B. McPherson, 2014, An Integrated Framework for Optimizing CO2 Sequestration and Enhanced Oil Recovery: Environmental Science and Technology Letters, v. 1, p. 49 – 54.

Gallagher, S. R., 2014, Depositional and diagenetic controls on reservoir heterogeneity: Upper Morrow Sandstone, Farnsworth Unit, Ochiltree County, Texas: Master's Thesis, New Mexico Institute of Mining and technology, Socorro, New Mexico, p. 215.

Garcia, J. E., 2001, Density of aqueous solutions of CO_2: Lawrence Berkeley National Laboratory. http://escholarship.org/uc/item/6dn022hb

Ingebritsen S. E., and M. S. Appold, 2012, The Physical Hydrogeology of Ore Deposits: Economic Geology, Bulletin of the Society of Economic Geologists, v. 107, no. 4, p. 559 – 584.

IPCC, 2005, IPCC special report on carbon dioxide capture and storage, prepared by Working Group III of the Intergovernmental Panel on Climate Change: Cambridge, United Kingdom and New York, NY, USA, Cambridge University Press, p. 442.

Johnson, K. S.; Amsden, T. W.; Denison, R. E.; Dutton, S. P.; Goldstein, A. G.; Rascoe, B., Jr.; Sutherland, P. K.; and Thompson, D. M., 1988, Southern Mid - continent region, in Sloss, L. L. (ed.), Sedimentary cover-North American craton, U.S.: The Geology of North America, Geological Society of America, Boulder, v. D-2, p. 307-359.

Johnson, K, S., 1989, Geologic evolution of the Anadarko Basin: Oklahoma Geological Survey Circular, v. 90, p. 3 – 12.

Johnson, J. W., E. H. Oelkers, and H. C. Helgeson, 1992, SUPCRT92: A software package for calculating the standard molal thermodynamic properties of minerals, gases, aqueous species, and reactions from 1 to 5000 bar and 0 to 1000°C: Computer and Geosciences, v. 18, no. 7, p. 899 – 947.

Liu, F., P. Lu, C. Zhu, Y. Xiao, 2011, Coupled reactive flow and transport modeling of CO2 sequestration in the Mt. Simon sandstone formation, Midwest, U.S.A. : International Journal of Greenhouse Gas Control, v. 5, p. 294 – 307.

Lorenz, S., and W. Müller, 2003, Modelling of halite formation in natural gas storage aquifers: Proceedings, TOUGH Symposium.

McKay, R. H., and J. T. Noah, 1996, Integrated perspective of the depositional environment and reservoir geometry, characterization, and performance of the Upper Morrow Buckhaults Sandstone in the Farnsworth Unit, Ochiltree County, Texas: Oklahoma Geological Survey Circular, v. 98, p. 101-114

Munson, T. W., 1988, Depositional, diagenetic, and production history of the Upper Morrowan Buckhaults Sandstone, Farnsworth Field, Ochiltree County Texas: Master's Thesis, West Texas University, Canyon, Texas, p. 117.

Munson, T,W., 1989, Depositional, diagenetic, and production history of the Upper Morrowan Buckhaults Sandstone, Farnsworth Field, Ochiltree County Texas: Oklahoma City Geological Society, Shale shaker, v. 40, no.13, p. 2 – 20.

Palandri J. L., and Y. K. Kharaka, 2004, A compilation of rate parameters of water – mineral interaction kinetics for application to geochemical modeling: U.S Geological Survey, Open file report 2004 – 1068.

Parker, R. L., 1956, "Farnsworth Morrow Oil Field": *The Panhandle Geonews*, v. 4, no. 1, p.5-12.

Pruess K., C. Oldenburg, G. Moridis, 1999, TOUGH2 user's guide, version 2.0. Lawrence Berkeley National Laboratory, Berkeley, CA, November, Rep LBNL – 43134.

Pruess, K., and J. Garcia, 2002, Multiphase flow dynamics during CO_2 disposal into saline aquifers: Environmental Geology, v. 42, no. 2 – 3, p. 282 – 295.

Pruess K., 2005, ECON2: A TOUGH2 fluid property module for mixtures of water, NaCl, and CO_2: Lawrence Berkeley National Laboratory, Paper: LBNL – 57592.

Spycher. N., and K. Pruess, 2005, $CO_2 – H_2O$ mixtures in the geological sequestration of CO_2. II. Partitioning in chloride brines at 12 – 100C and up to 600 bar: Geochimica et Cosmochimica Acta, v. 69, no. 13, p. 3309 – 3320.

Swanson, D. C., 1979, Deltaic deposits in the Pennsylvanian upper Morrow Formation of the Anadarko basin, in Hyne, N. J. (ed.), Pennsylvanian sandstones of the Mid – Continent: Tulsa Geological Survey Special Publication, v. 1, p. 115 – 168.

US Environmental Protection Agency, 2012, Inventory of US greenhouse gas emissions and sinks 1990–2010. Report EPA 430-R-12-001, Washington.

White, M.D., B. J. McPherson, R.B. Grigg, W. Ampomah, and M. S. Appold, 2014, Numerical Simulation of Carbon Dioxide Injection in the Western Section of the Farnsworth Unit: Energy Procedia, v. 63, p. 7891 – 7912.

Xu, T., J. A. Apps, K. Pruess, 2004, Numerical simulation of CO_2 disposal by mineral trapping in deep aquifers: Appl. Geochem, v. 19, p. 917 – 936.

Xu, T., J. A. Apps, K. Pruess, 2005, Mineral sequestration of carbon dioxide in a sandstone – shale system, Chemical Geology, v. 217, p. 295 – 318.

Zhu, C., and D. S. Burden, 2001, Mineralogical compositions of aquifer matrix as necessary initial conditions in reactive contaminant transport models: Journal of Conaminant Hydrology, V. 51, p. 145 – 161.

Figures

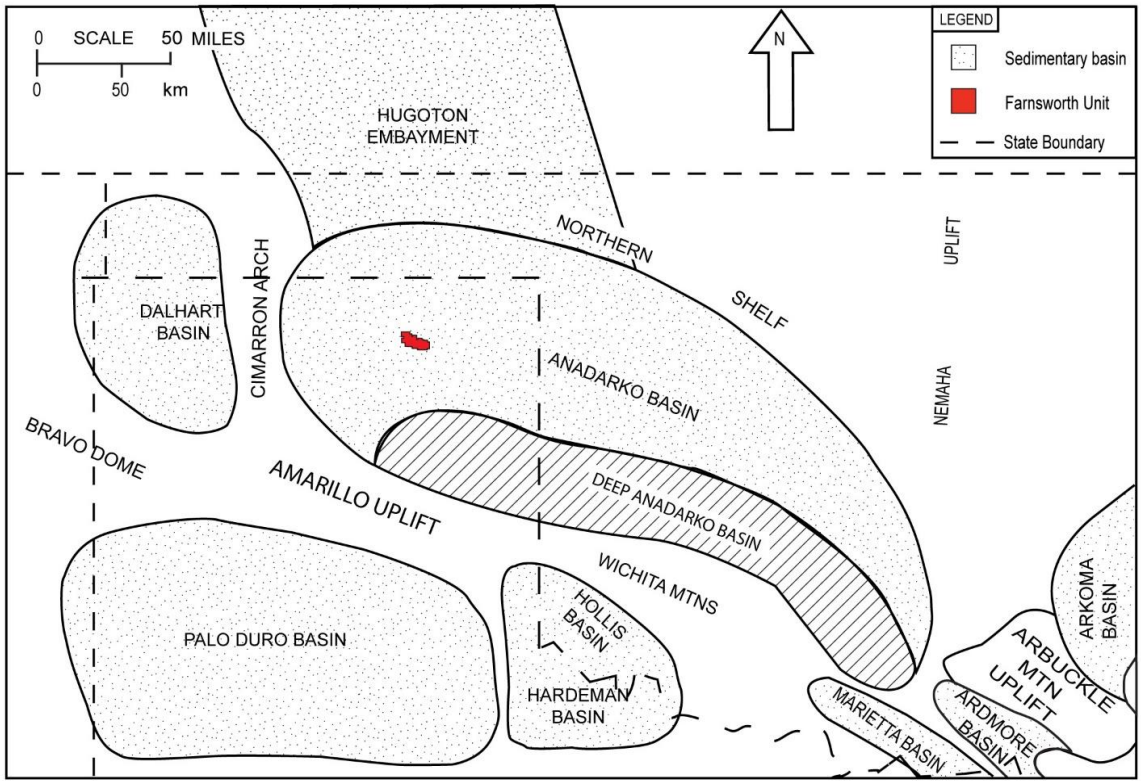

Figure 11: Geologic context and location of the Farnsworth Unit (modified after Johnson et al., 1988).

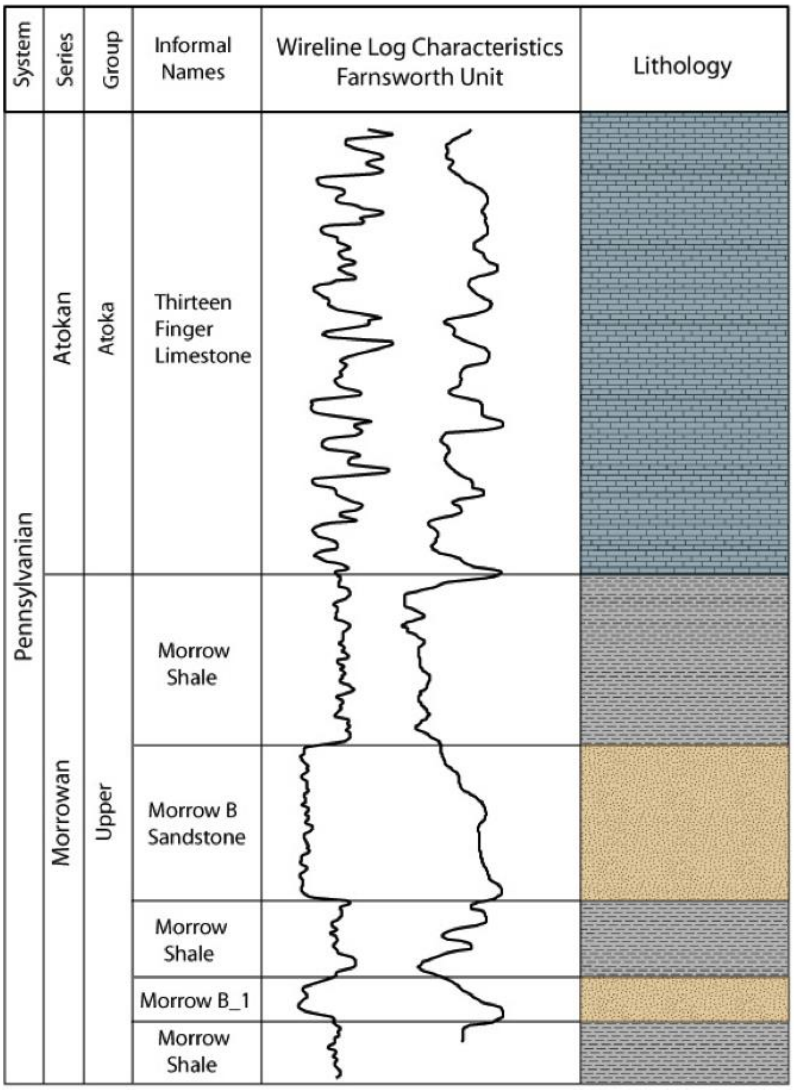

Figure 12: Stratigraphic chart showing divisions of the Upper Morrowan and Lower Atokan-aged strata in the Farnsworth Unit. Wireline log is from well 32-2. Modified from Munson (1989) and Puckette et al. (2008) by Gallagher (2014).

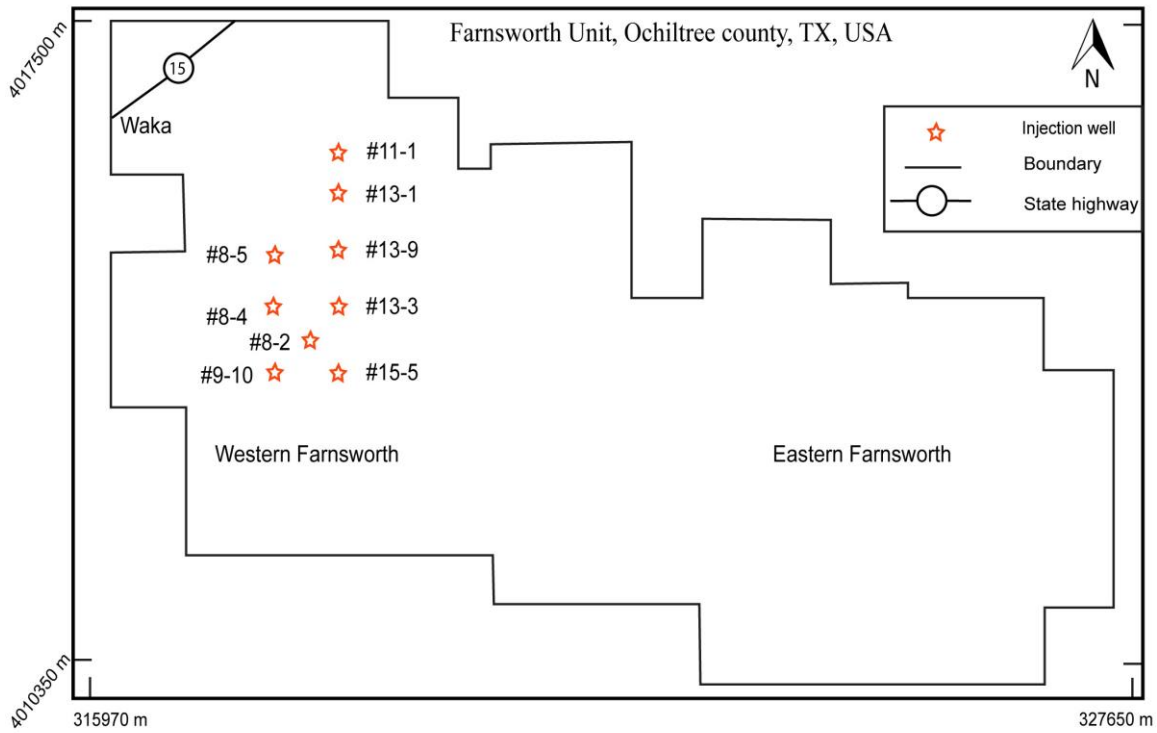

Figure 13: Plan view of the Farnsworth Unit showing locations of CO_2 injection wells.

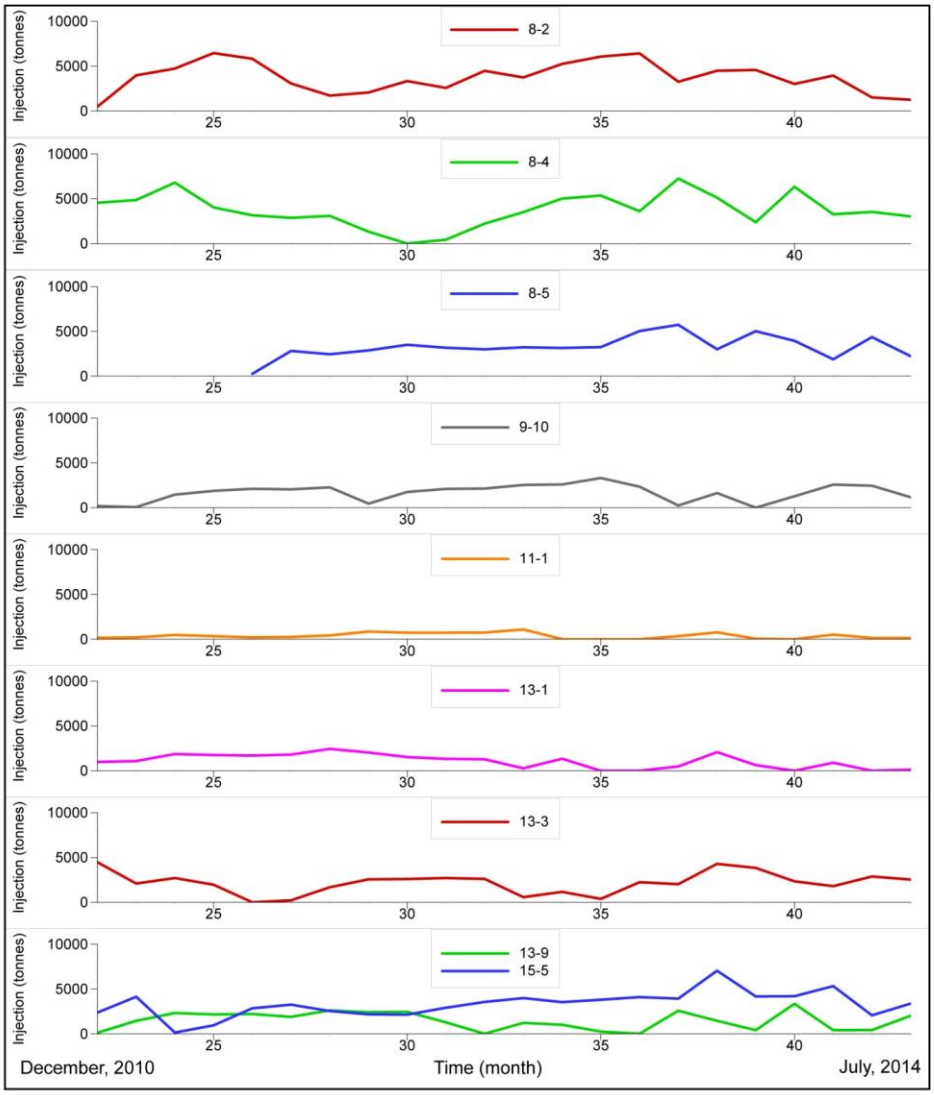

Figure 14: CO_2 injection schedules for wells shown in Figure 13.

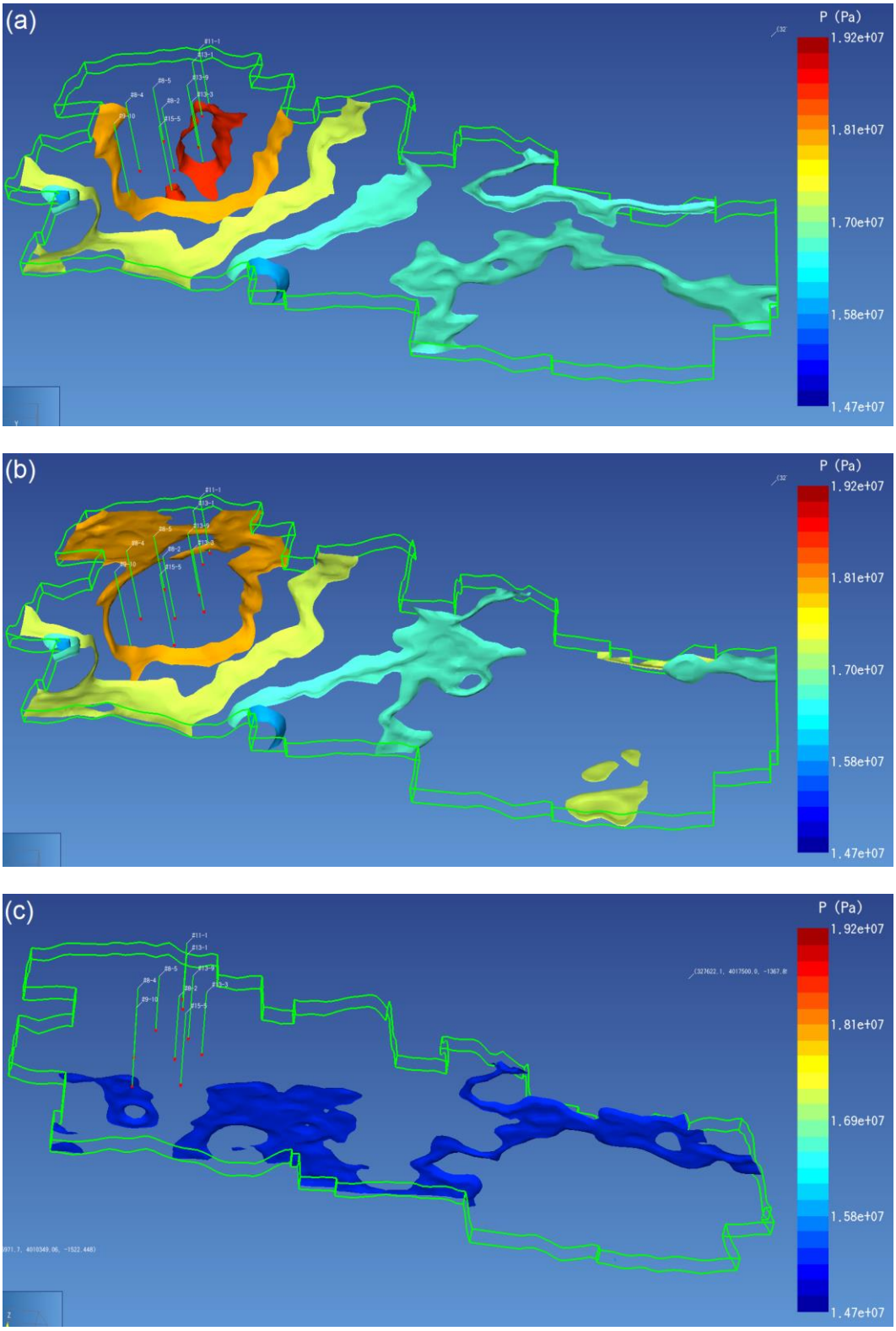

Figure 15: Isosurface plots showing pore fluid pressure after (a) 1 year, (b) 10 years, and (c) 30 years of simulation time.

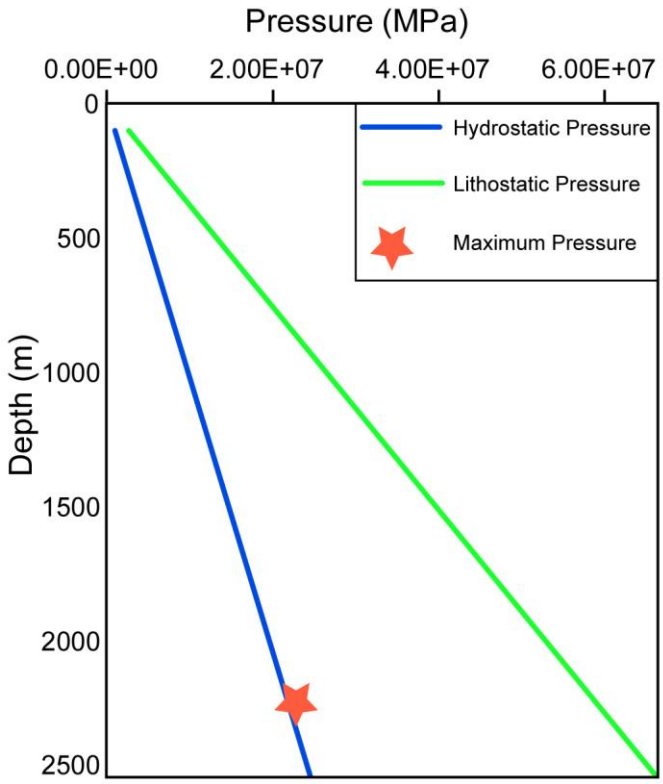

Figure 16: Plot showing the maximum pore fluid pressure reached in the Farnsworth Unit as a result of CO_2 injection. The maximum pressure is well below the lithostatic pressure by which failure of the reservoir matrix would be expected to occur.

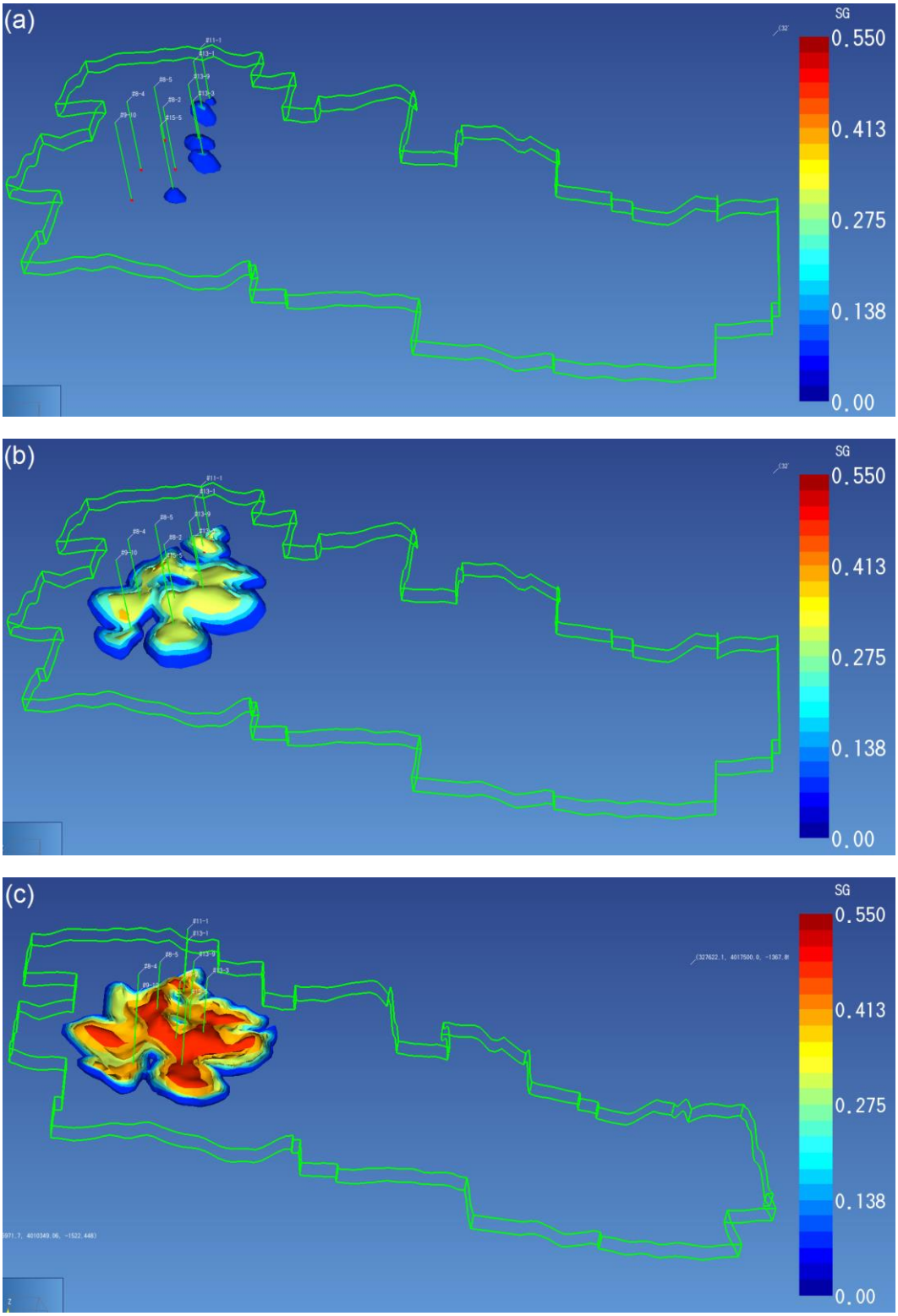

Figure 17: CO_2 gas saturation (fraction) after (a) 1 year, (b) 10 years, and (c) 30 years of simulation time.

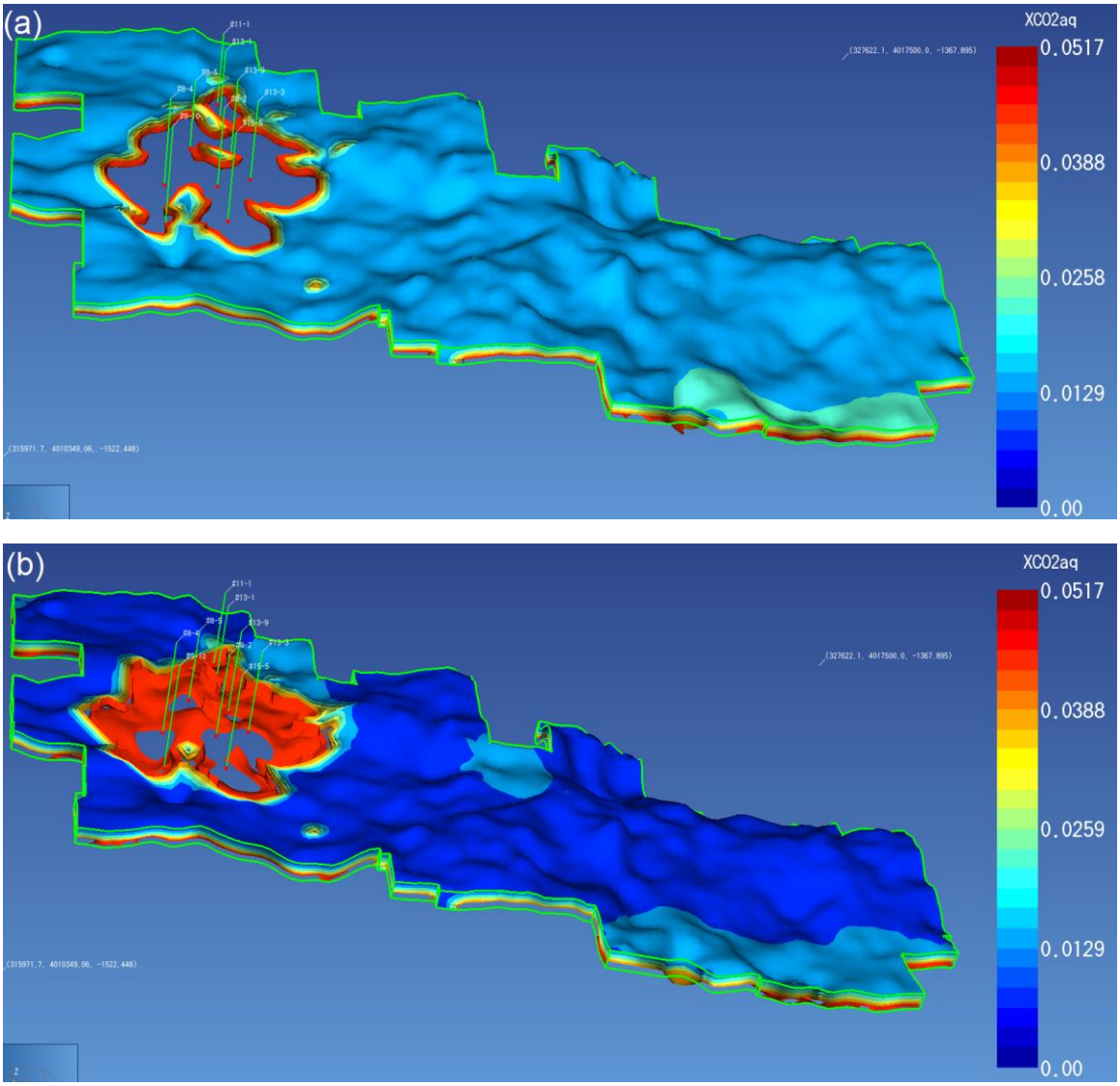

Figure 18: Concentration of aqueous CO_2 after (a) 10 years and (b) 30 years.

(The blank gray space around the wells in the left part of the plot represents maximum aqueous CO_2 concentrations, i.e. 0.052 m.)

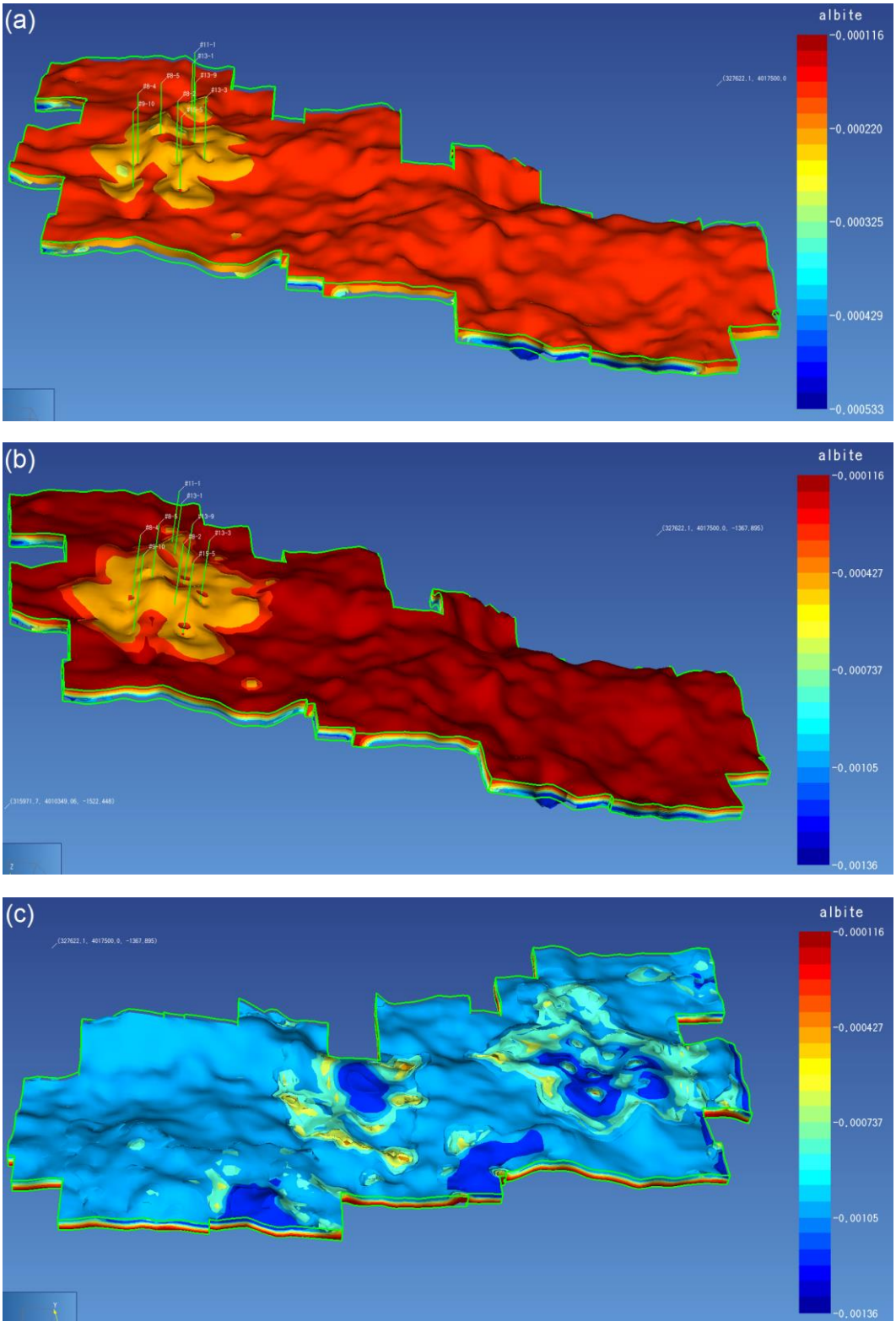

Figure 19: Predicted change in the volume fraction of albite as viewed from the top of the grid after (a) 10 years (b) 30 years and (c) as viewed from the bottom of the grid after 30 years of simulation time.

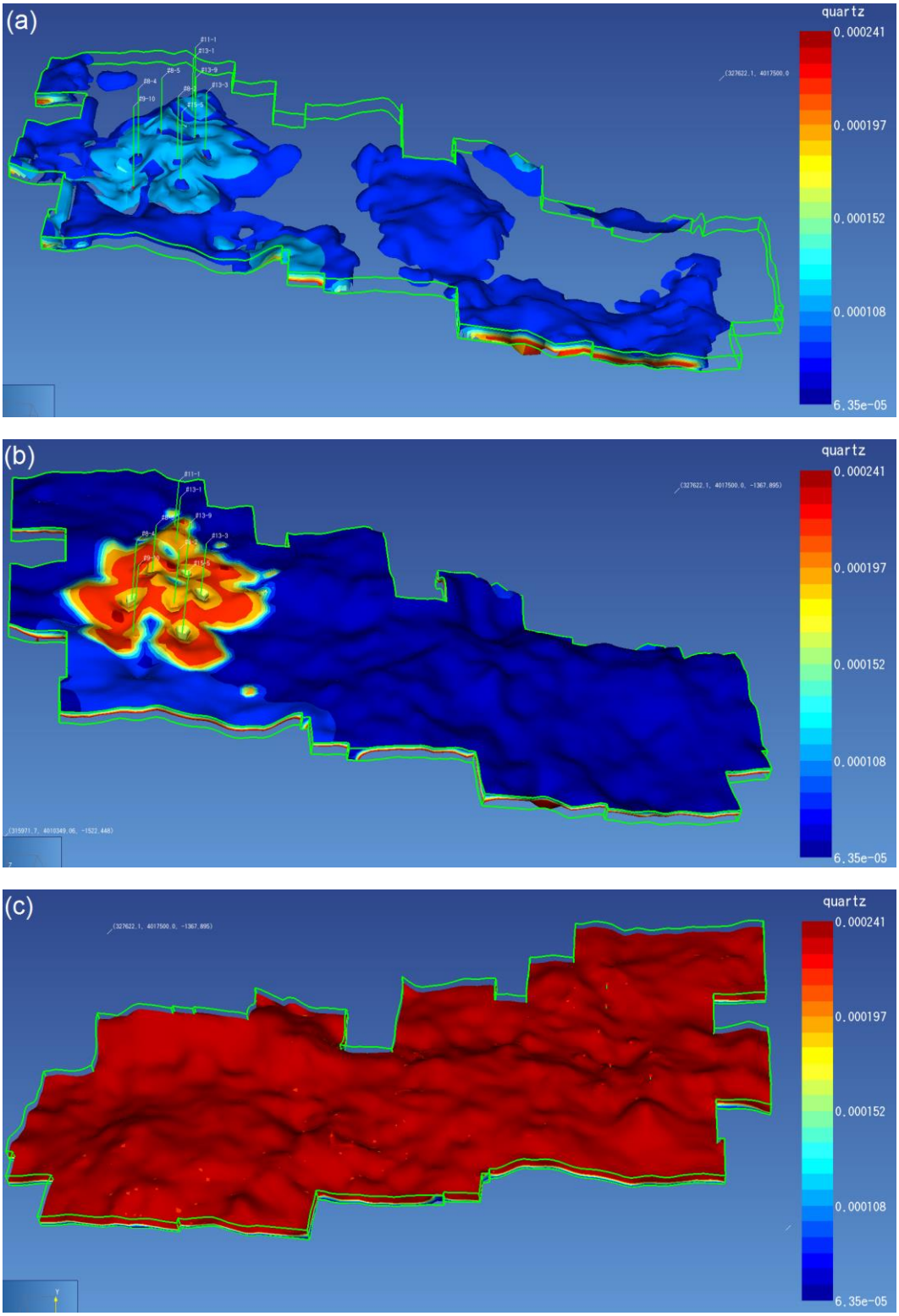

Figure 20: Predicted change in the volume fraction of quartz as viewed from the top of the grid after (a) 10 years (b) 30 years and (c) as viewed from the bottom of the grid after 30 years of simulation time.

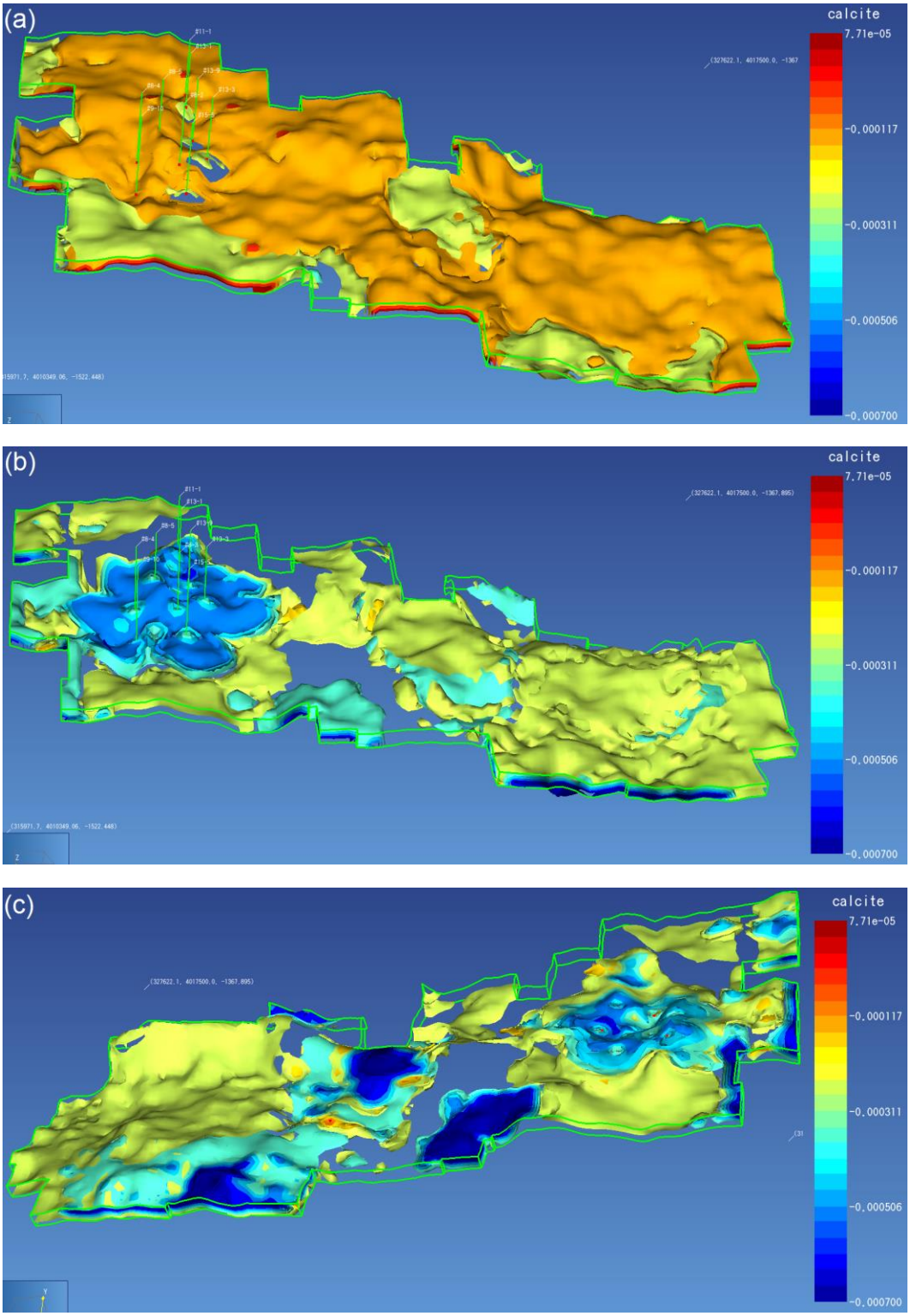

Figure 21: Predicted change in the abundance of calcite as viewed from the top of the grid after (a) 10 years (b) 30 years and (c) as viewed from the bottom of the grid after 30 years of simulation time.

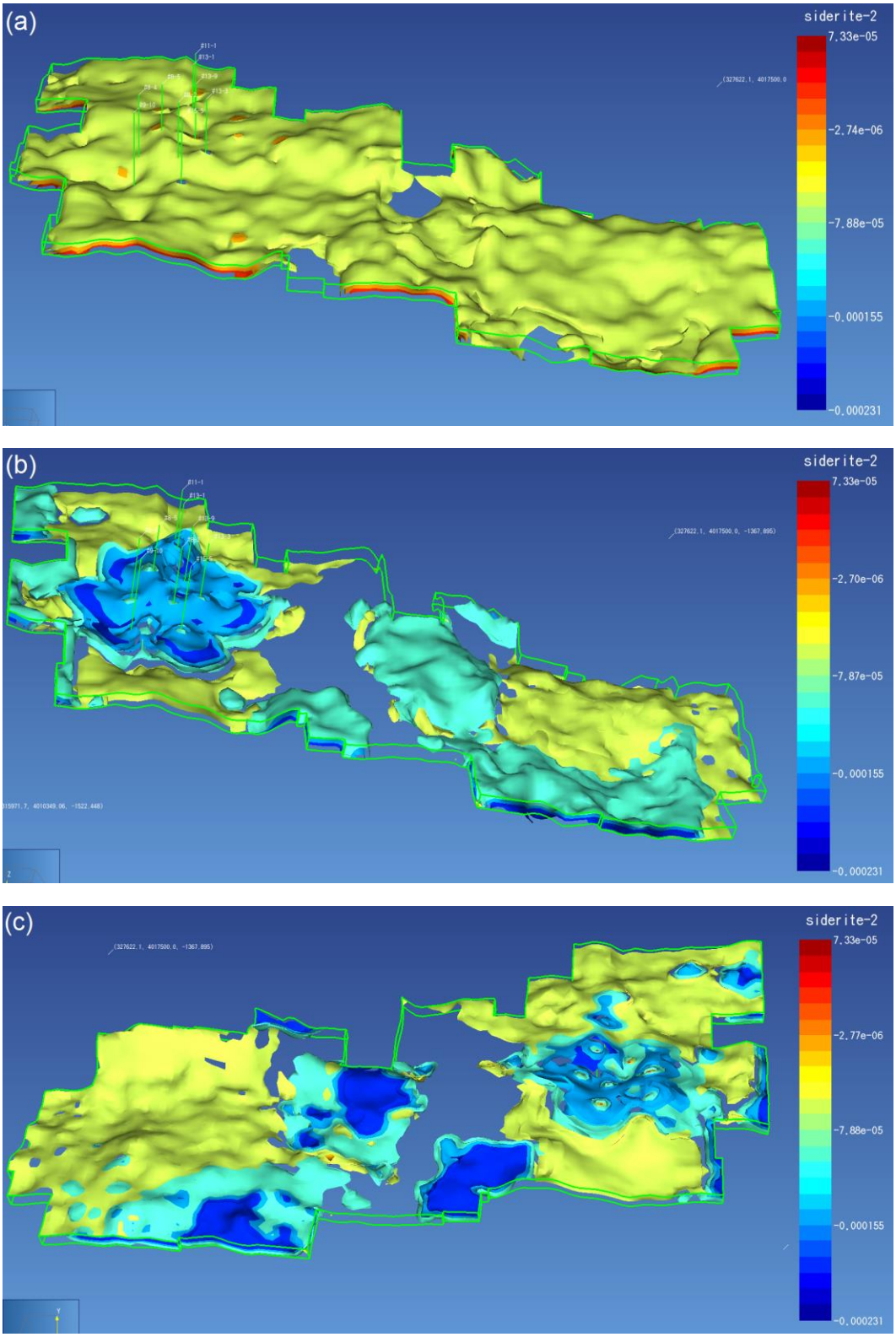

Figure 22: Predicted change in the volume fraction of siderite as viewed from the top of the grid after (a) 10 years (b) 30 years and (c) as viewed from the bottom of the grid after 30 years of simulation time.

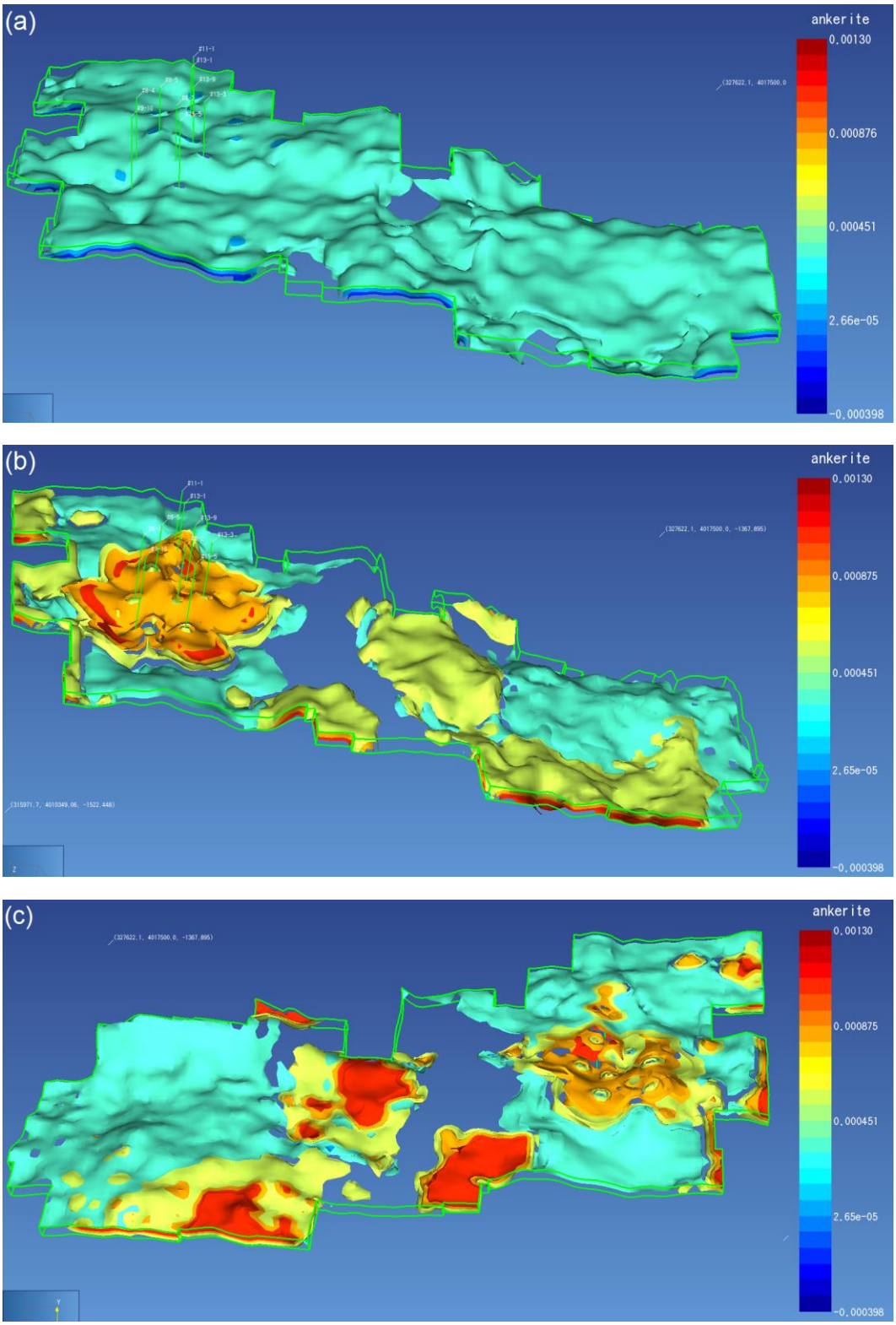

Figure 23: Predicted change in the volume fraction of ankerite as viewed from the top of the grid after (a) 10 years (b) 30 years and (c) as viewed from the bottom of the grid after 30 years of simulation time.

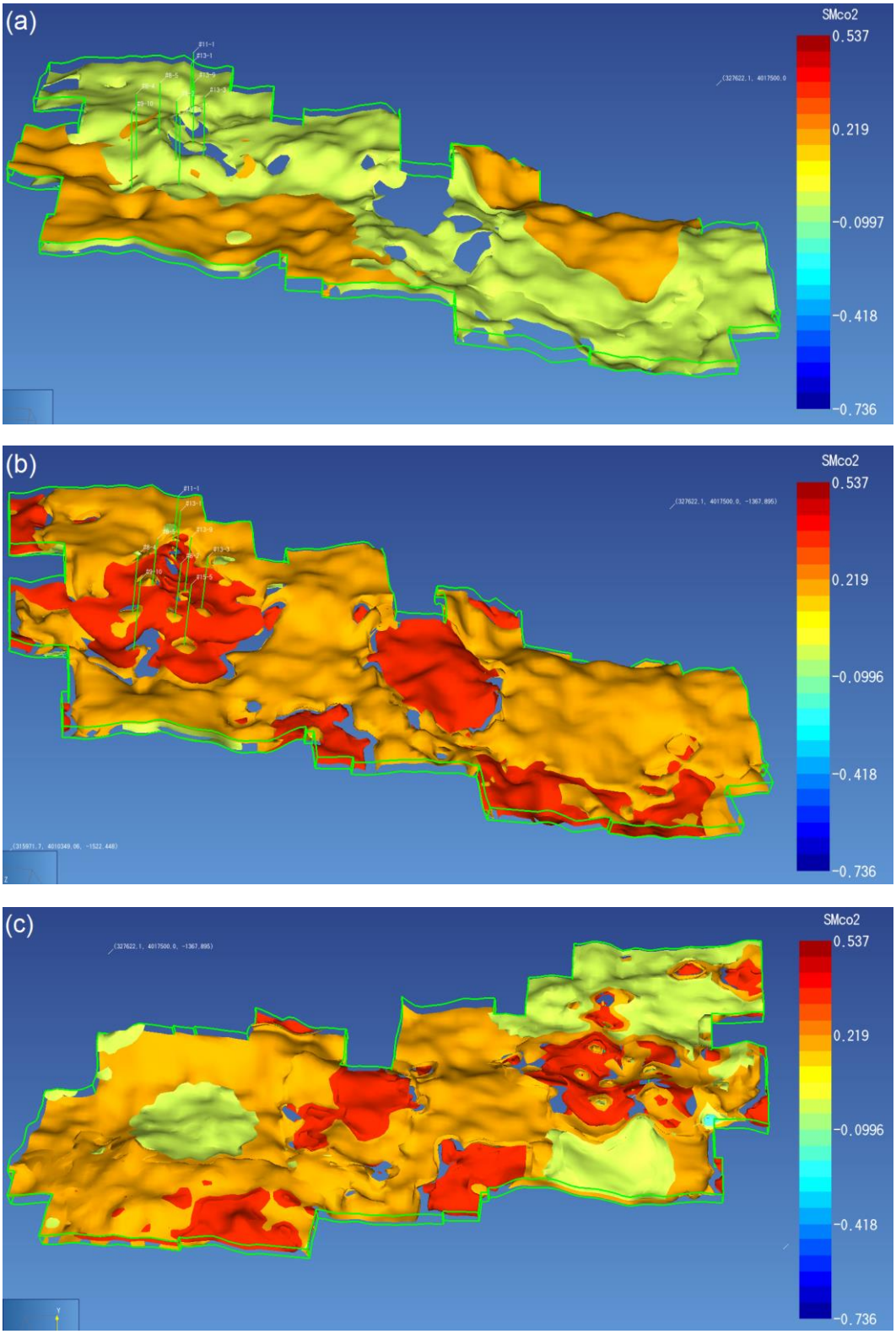

Figure 24: Predicted mass of CO_2 sequestered as minerals per grid cell volume (kg/ m^3 medium) as viewed from the top of the grid after (a) 10 years (b) 30 years and (c) as viewed from the bottom of the grid after 30 years of simulation time.

Tables

Table 3: Model composition of Morrow B pore water

Basis Species	Fluid concentration mg/kg
Al^{+++}	0.52
$B(OH)_{3(aq)}$	24.65
Ba^{++}	0.981
Br^{-}	19.05
Ca^{++}	35.7
Cl^{-}	1655
F^{-}	0.7825
Fe^{++}	3.65E-05
HCO_3^{-}	674
K^{+}	7.49
Li^{+}	0.461
Mg^{++}	12.3
Na^{+}	1245
SO_4^{2-}	17.15
SeO_3^{2-}	0.0757
$SiO_{2(aq)}$	33.3
Sr^{++}	2.265
Zn^{++}	0.054
pH	7

Table 4: Initial mineral composition of the Morrow B sandstone.

Mineral	**Volume (%)**
Quartz	84.26
Anorthite	4.5
Albite	4.5
Chlorite	1.785
Kaolinite	2.72
Mont	0.1
Illite	0.88
Siderite	0.25
Ankerite	0.25
Calcite	0.75
magnesite	0
dolomite	0

Table 5: Well identifications with their corresponding coordinates, screen depths, and fluid enthalpies.

Well	X (m)	Y (m)	Screen depth (m)	Fluid enthalpy (J/kg)
8#2	318194.3	4014437	5	562500
8#4	317753.5	4014483	5	562500
8#5	317856.9	4015004	5	562500
9#10	317783.6	4013821	5	562500
11#1	318612.7	4016074	5	562500
13#1	318607.7	4015651	5	562500
13#3	318604	4014450	5	562500
13#9	318608.5	4015053	5	562500
15#5	318578.9	4013679	5	562500

Table 6: Matrix of model rock types and their corresponding porosity and permeability values.

Porosity / Permeability	0	>0 – 0.1	>0.1 – 0.125	>0.125 – 0.15	>0.15 – 0.2	>0.20
1×10^{-17}	Rock1					
$> 1 \times 10^{-17}$ - 2.46×10^{-14}		Rock2	Rock3	Rock4	Rock5	Rock6
$> 2.46 \times 10^{-14}$ – 4.93×10^{-14}		Rock7	Rock8	Rock9	Rock10	Rock11
$> 4.93 \times 10^{-14}$ -7.4×10^{-14}		Rock12	Rock13	Rock14	Rock15	Rock16
$>7.4 \times 10^{-14}$ – 9.87×10^{-14}		Rock17	Rock18	Rock19	Rock20	Rock21
$>9.87 \times 10^{-14}$ – 1.23×10^{-13}		Rock22	Rock23	Rock24	Rock25	Rock26
$>1.23 \times 10^{-13}$ – 1.48×10^{-13}		Rock27	Rock28	Rock29	Rock30	Rock31
$>1.48 \times 10^{-13}$ - 1.72×10^{-13}		Rock32	Rock33	Rock34	Rock35	